ALMA Memo 609

Effects of Direct IF Sampling on the Time-Division Multiplexing Mode of Operation of the ALMA Correlator

Omar A. Yeste Ojeda, January 2018

List of acronyms and abbreviations

ADC	Analog-to-Digital Converter
ALMA	Atacama Large Millimeter Array
DIFS	Direct IF Sampling
FDM	Frequency-Division (Multiplexing) mode
FFT	Fast Fourier Transform
FIR	Finite Impulse Response
FPGA	Field-Programmable Gate Array
IF	Intermediate Frequency
IFFT	Inverse Fast Fourier Transform
LO	Local Oscillator
LSB	Least Significant Bit
PDF	Probability Density Function
PFB	Polyphase Filter Bank
RMS	Root Mean Square
TDM	Time-Division (Multiplexing) mode
TFB	Tunable Filter Bank

Abstract

This document reports on some of the effects that using Direct IF (Intermediate Frequency) Sampling (DIFS) at the receiver's backend would have on the correlator's Time-Division Multiplexing mode (TDM). Specifically, a slight degradation in the quantization efficiency and required implementation changes of TDM are described. The immediate cause lies in the need for a digital frequency converter after the Analog-to-Digital Converter (ADC) to compensate for the removal of the receiver's second Local Oscillator (LO).

1 Introduction

The current Atacama Large Millimeter Array (ALMA) 64-antenna correlator can operate as an XF correlator (TDM) or as a hybrid FXF correlator (Frequency-Division Multiplexing mode, or FDM). TDM is mostly used for continuum observations and standard setups such as pointing, focus, delay calibration, system temperature measurements, sideband ratio measurements, etc. [1]. In TDM, the full bandwidth (currently 2 GHz) is directly sent to the correlator, bypassing the

Tunable Filter Bank (TFB). As the correlator admits 2 or 4-bit inputs, the Least Significant Bit (LSB) of the 3-bit ADC samples must be discarded in the 2-bit correlator case.

On the other hand, progress on ADC technology makes DIFS, whereby one ultra-fast ADC digitizes the entire IF bandwidth, not only interesting but also practical. This approach notably simplifies the backend but eliminates the second analog frequency conversion, which must now be done digitally (e.g., for fine fringe tracking or LO offsetting). This frequency conversion can be integrated with the digital frequency conversion carried out within the TFB, which is currently used only in FDM. More details on this possibility can be found in Section 0, after the quantization efficiency analysis.

The digital frequency conversion causes a growth of the number of bits per sample, hence demanding a second quantization before the signal can be fed into the correlator. As a consequence, the sensitivity loss of TDM increases. The purpose of Section 3 is to quantify the quantization efficiency of TDM when a digital frequency conversion is carried out. The results are developed using some simplifications, such as flat spectrum and perfect delay tracking and fringe rotation. Additional effects, such as the sensitivity loss due to center frequency displacement [2], are not considered.

2 Signal model and approximations

Consider the simplified architecture represented in Figure 1. The IF signal is assumed stationary, Gaussian, zero-mean, and bandpass. The signal spectrum is approximated as flat in the pass band, and is critically sampled by the ADC, so that samples are statistically independent from each other. In practice, the extreme of the pass band should fall by effect of the anti-aliasing filter. This is used as a justification for approximating the frequency conversion process as lossless, by considering negligible the aliasing effect if the signal is shifted in frequency by a small amount. As a result, the output of the frequency converter can be expressed as[1]:

$$x(n) = z(n)\ \cos(\omega n + \varphi) \mp \hat{z}(n)\ \sin(\omega n + \varphi) \qquad (1)$$

where $z(n)$ is the ADC output, $\hat{z}(n)$ its Hilbert transform, $\omega = 2\pi f$, f is the frequency shift, φ is an arbitrary phase, and the minus sign applies to up-conversion (while the plus sign applies to down-conversion).

The output of the ADC follows a discrete distribution. However, its Hilbert transform is approximately Gaussian by virtue of the central limit theorem. Moreover, the two samples $z(n)$

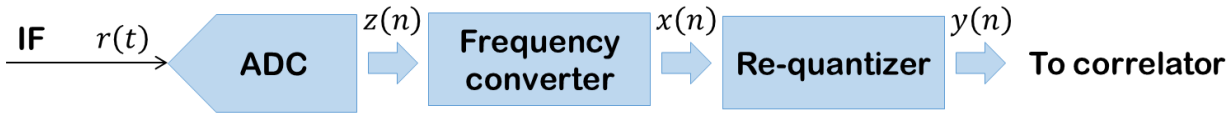

Figure 1. Simplified TDM architecture under study throughout this document

[1] An infinite precision frequency converter is used, assuming the precision of its implementation is high, which is required for accurate tunability.

and $\hat{z}(n)$ (i.e., at a specific instant n) are statistically independent provided that $z(n)$ is a sequence of independent samples, as was assumed[2].

As a result, the Probability Density Function (PDF) of $x(n)$ is periodically time-dependent, oscillating from discrete to Gaussian, and the convolution of both (a Gaussian mixture) in the general case. Therefore, the quantization efficiency also varies with time. However, the sensitivity will depend on the average efficiency, given that the correlator integration time either comprises an integer number of periods, or is much greater than one period. In any case, the quantization efficiency will always be bounded by the current value for TDM, attained at instants when the cosine in (1) is 1, and the value for FDM, obtained when the cosine is zero.

3 Results

Appendix A develops the method used to compute the quantization efficiency of a cross-correlation estimate when the frequency and phase of the frequency converter are the same for the two signals being correlated. A more general but less accurate method is described in Appendix B, which can be used for validation purposes. In all cases, and for both the ADC and the re-quantizer, a uniform quantization function is used, with equal size steps and output values assigned linearly, that is $\{\pm 0.5, \pm 1.5, \pm 2.5, \dots\}$. Results show three different cases wherein there is a significant variation of the efficiency, depending on whether none, one or both signals are digitally frequency shifted[3]. These three cases are considered separately in the following:

3.1 No frequency converter

This case requires fringe tracking to be performed entirely by the first local oscillator. Thus, LO offsetting (e.g., for sideband suppression [1]) is not allowed, as the IF outputs from all antennas corresponding to a given sky frequency band the front-ends must be aligned in frequency at the ADC input.

Consider the current 3-bit ADC and 2-bit correlator. Figure 2 represents the overall quantization efficiency as a function of the ADC quantization step (in input's Root Mean Square (RMS) units) and the re-quantization step (for ADC output values $\{\pm 0.5, \pm 1.5, \pm 2.5, \dots\}$). No frequency shift is applied prior to the re-quantization of the signal, and hence this case represents the current TDM. As expected, the maximum efficiency corresponds to that of 2-bit quantizer, i.e., 88.115% [3], and can be achieved in three different ways: Using the optimal 2-bit quantization step at the ADC (0.996) and then a re-quantization step around 1 (the exact value is not important due to the discrete nature of the re-quantizer input); halving the ADC step while doubling the re-quantization step; or dividing the optimal ADC step by 3, and then using a re-quantization step about 3. All these results are well-known and serve as a reference for the following cases.

3.2 Both basebands are shifted in frequency

This is the common case when the ADC inputs are not aligned in frequency. In this case, LO offsetting is allowed for sideband and spurious suppression, fine fringe tracking can be carried

[2] This is straightforward from the Hilbert transform implementation as a non-causal IIR filter, whose impulse response is zero at lag zero.

[3] With reference to (1), it is assumed that $\varphi = 0$ if $f = 0$.

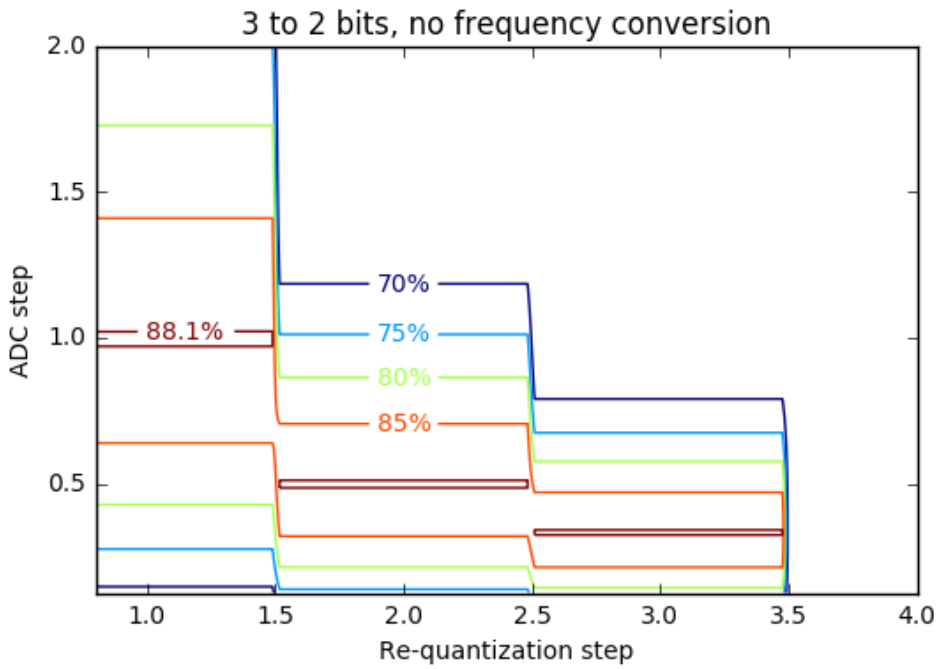

Figure 2. Overall quantization efficiency using a 3-bit ADC and a 2-bit correlator. No frequency shift is performed on the baseband pair.

out digitally. The quantization efficiency is quite independent from the frequencies and phases utilized in the frequency conversion[4]. Figure 3 represents the quantization efficiency as a function of the ADC and re-quantization steps. The maximum efficiency, 85.364%, is smaller than what obtained in the previous case, but higher than the maximum that could be obtained through FDM, 84.816%. A single maximum is obtained at an ADC quantization step 0.529, which locates between the optima for TDM ($0.996/2 = 0.498$) and FDM (0.586) [3]. The re-quantization step for maximum efficiency is 1.863, which is slightly higher than the optimal step, 1.801, at the instants when the frequency converter output follows a Gaussian distribution.

3.3 Only one baseband is shifted in frequency

This case may arise when a master antenna is taken as a reference to compensate for the different phase/delay from the other antennas. The same considerations as in the previous case can be done. The quantization efficiency in this case can be accurately approximated as the geometric mean of the two previous cases. As an example, Figure 4 shows the quantization efficiency when both basebands are quantized using the same quantization steps. The maximum efficiency in this case is 86.711%, for an ADC quantization step 0.511, and a re-quantization step 1.899. If different quantization steps were allowed, the geometric mean of the maxima in the two previous cases would become 86.729%, an improvement too small to justify the increased complexity.

[4] As long as the distribution of samples of the sinusoid (cosine and sine) terms in (1) corresponding to a correlator integration interval is representative of a sinusoid function. For example, this is not satisfied if the sinusoid period is a short integer number. For small frequency shifts (relative to sampling frequency), this condition is satisfied. More details can be found in Appendix D.

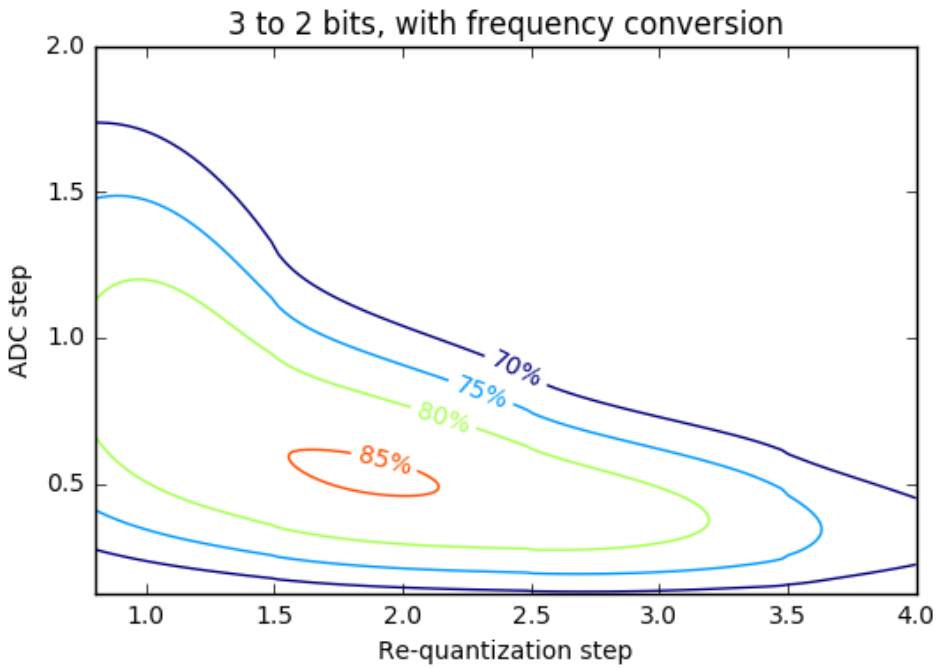

Figure 3. Overall quantization efficiency using a 3-bit ADC and a 2-bit correlator. Both basebands are frequency shifted prior to re-quantization. The maximum efficiency is 85.36%.

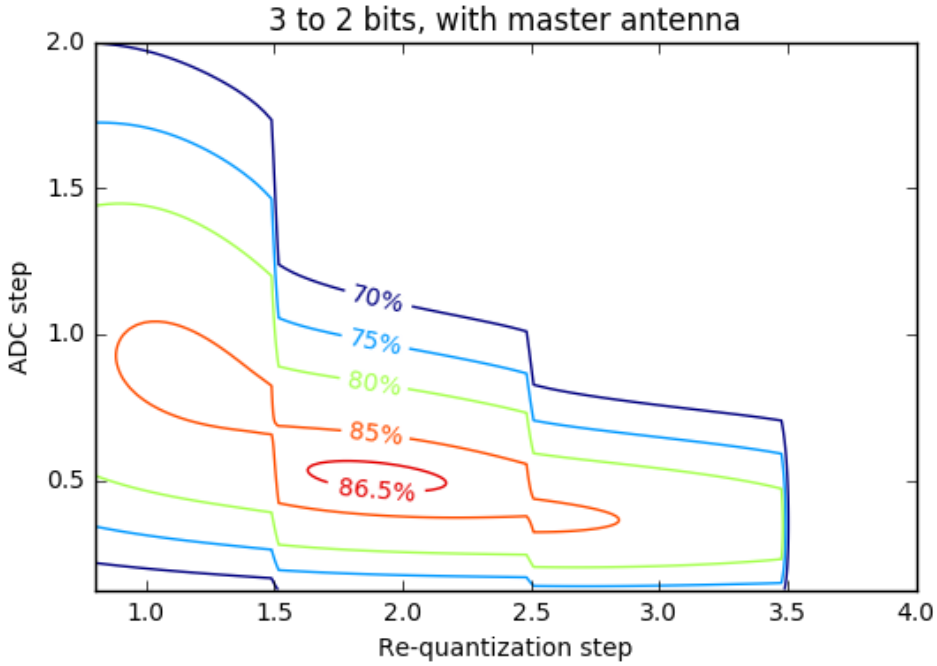

Figure 4. Overall quantization efficiency using a 3-bit ADC and a 2-bit correlator. Only one baseband is shifted in frequency after the ADC. The maximum efficiency is 86.71%.

TABLE 1. QUANTIZATION EFFICIENCY FOR A 3-BIT ADC AND A 2-BIT CORRELATOR

Mode	ADC step	Re-quant. step	Basebands shifted	Efficiency
TDM	0.996, 0.498, 0.332	1.0, 2.0, 3.0	—	88.115 %
TDM with a frequency converter	0.529	1.863	None	88.031 %
			One	86.687 %
			Both	85.364 %
FDM	0.586	1.801	—	84.816 %

TABLE 2. QUANTIZATION EFFICIENCY FOR A 3-BIT ADC AND A 4-BIT CORRELATOR

Mode	ADC step	Re-quant. step	Basebands shifted	Efficiency
TDM	0.586	1.0	—	96.256 %
TDM with a frequency converter	0.579	0.553	None	95.712 %
			One	95.481 %
			Both	95.249 %
FDM	0.586	0.561	—	95.145 %

To summarize, Table 1 gathers the quantization efficiency for fixed quantization steps[5] and compares them to current TDM and FDM. The results for a 4-bit correlator (see Table 2) are qualitatively very similar, except that there is only one global maximum for TDM. More details on results for the 4-bit correlator are provided in Appendix C.

4 Some implementation considerations

The first practical issue that arise from (1) is how to implement a Hilbert transformer. This is the same problem as producing the discrete analytic signal from a discrete real-valued signal. Three of the most popular solutions are [4]: using the DFT (impractical for real-time, very long sequences), using a Finite Impulse Response (FIR) approximation to a discrete Hilbert filter, or low-pass filtering the product of the input signal and a complex exponential. This last approach seems preferable [4], even more as its similarities with FDM (a complex frequency conversion followed by a low-pass filter) might enable resource sharing between TDM and FDM.

Then, the implementation of the architecture in Figure 1 becomes as shown in Figure 5, which is very similar to the TFB used in FDM (cf. Figure 2 in [5]). The main differences relate to

[5] The quantization step has been chosen to maximize the minimum efficiency, i.e., the one for the case when both basebands have been shifted in frequency.

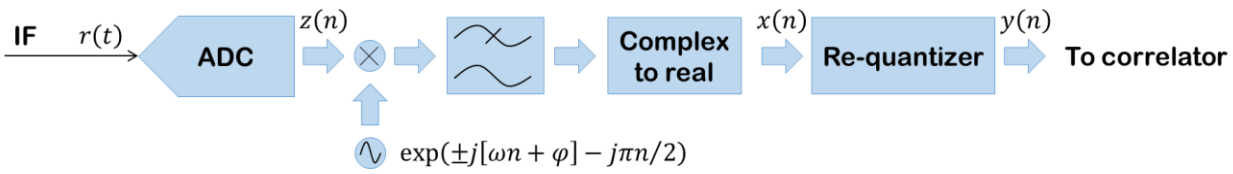

Figure 5. One possible implementation of the frequency converter.

the low-pass filter, which does not decimate in TDM and whose bandwidth equals the Nyquist frequency.

Whereas the ADC sampling rate is higher than the Field-Programmable Gate Array (FPGA) clock where most likely the frequency converter would be implemented, both the input and output of the low-pass filter in Figure 5 consist of parallel data streams. For example[6], a sampling rate of 8 GHz and an FPGA clock frequency of 250 MHz would lead to 32 parallel data streams. In addition, the number of taps of the filter needs to be in the order of several hundreds to minimize sensitivity loss in the passband. Thus, Fast Fourier Transform (FFT)-based filtering methods (e.g., overlap-save or overlap-add) seem the most suitable ones for the implementation of the low-pass filter. The number of filter taps can be made as large as $L = F - R + 1$, where F is the FFT length and R is the overlap, i.e., the ratio between the ADC and FPGA clocks. For example, with a 1024-point FFT, a 993-tap filter can be designed for an overlap of 32 samples. An example of such a filter is shown in Figure 6.

Two final observations can be made regarding this implementation of TDM. First, finer delay tracking can be readily achieved by properly adjusting the group delay of the filter response. Special care should be taken when implementing real-time operation in the most efficient way. Second, as the practical implementation of the Hilbert transformer is inherently bandpass, the PDF of the re-quantizer input cannot reach a discrete distribution, and becomes more similar to a Gaussian one. This effect becomes more pronounced if the group delay is not an integer number of samples, for example, so that a finer delay tracking can be performed. It is noteworthy that the more Gaussian the re-quantizer input is, the closer the quantization efficiency will be to that of FDM.

4.1 Integration with FDM

From the example in Figure 6, it seems that shorter FFTs can still satisfy the filter requirements. However, it might be advantageous that FDM and TDM share one FFT core and that the length of the FFT be determined by the implementation of FDM. Currently, the TFB for each station is implemented by a single card using 16 FPGAs [5]. However, an upgraded TFB can be more efficiently implemented in a single FPGA. Then, there is a flexibility vs. resource cost trade-off in the implementation of the TFBs: from the current design wherein each sub-band can be independently tuned with 30.5-KHz resolution, to a Polyphase Filter Bank (PFB)-based implementation with fixed sub-band locations. One possible compromise would consist in removing the frequency decimation feature of PFBs and compute the entire N-point FFT, where N is the PFB filter length. A switch matrix at the output would select which FFT channels

[6] There is no intention to propose or set any implementation parameter in this document.

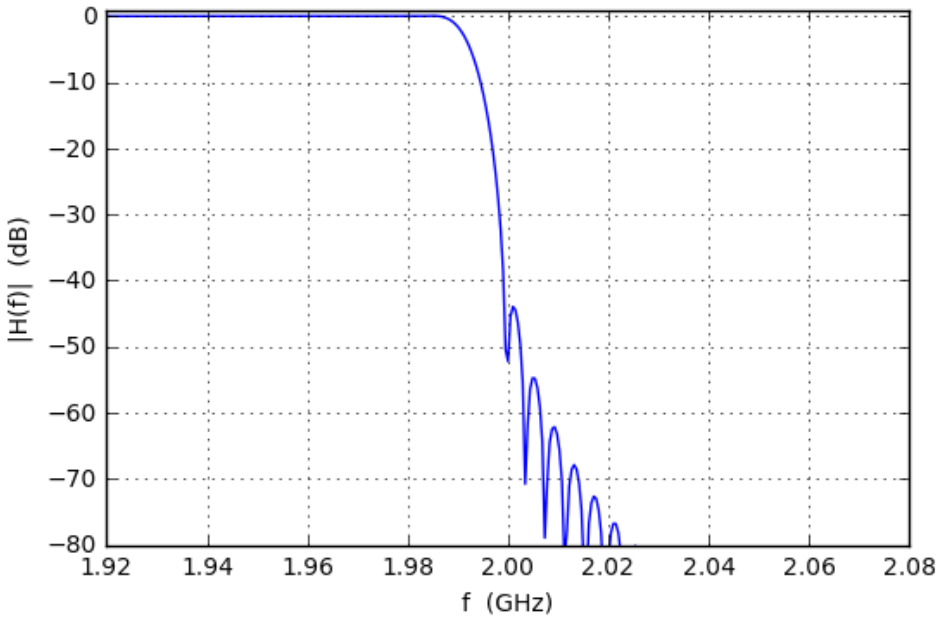

Figure 6. Transition band of an exemplary 933-tap filter at 4-GHz sampling rate. The frequency axis has been shifted by 1GHz for a more meaningful comparison to the current ALMA system.

constitute the set of sub-bands. Thus, the FFT size would be determined by the desired tunability of FDM sub-bands.

An example of such a TFB configuration for 1024-point FFT and 4-GHz sampling rate is shown in Figure 7. As in the current ALMA correlator, 32 sub-bands with 62.5-MHz bandwidth each are computed. The current ALMA spectral configuration [1] can be obtained through a sub-band spectral separation of 15 FFT bins. Figure 7-a illustrates the trade-off between in-band loss and aliasing rejection at the spectral channels near the sub-band boundaries for a 1024-tap filter. At the channel boundary, the in-band loss is 2.65 dB, while the aliasing attenuation is 11.6 dB, resulting into an aliasing rejection of 9.0 dB for the aliased components. There are two ways to improve these figures: The first one consists of reducing the spectral separation between sub-bands at the cost of decreasing the spectral window. This has been represented in Figure 7-a with dashed lines for a sub-band separation of 14 FFT bins, yielding 0.84 dB in-band loss and 19.8 dB aliasing rejection. The second way is more effective way and consists of increasing the FFT window through a PFB. In this second approach, the price is paid in terms of computational burden. An example using a 4-tap PFB is represented in Figure 7-b, attaining 0.05 dB in-band loss and 44.0 dB aliasing rejection.

In summary, the cost of implementing the frequency converter required in TDM to compensate for the removal of the second LO can be alleviated by sharing part of the resources with FDM. An example of joint implementation is shown in Figure 8. In this example, both modes share the first finely tunable complex frequency converter and a (1024-point) FFT. In TDM, the PFB is bypassed. The FFT output is then processed differently in each mode. In FDM, 32 out of

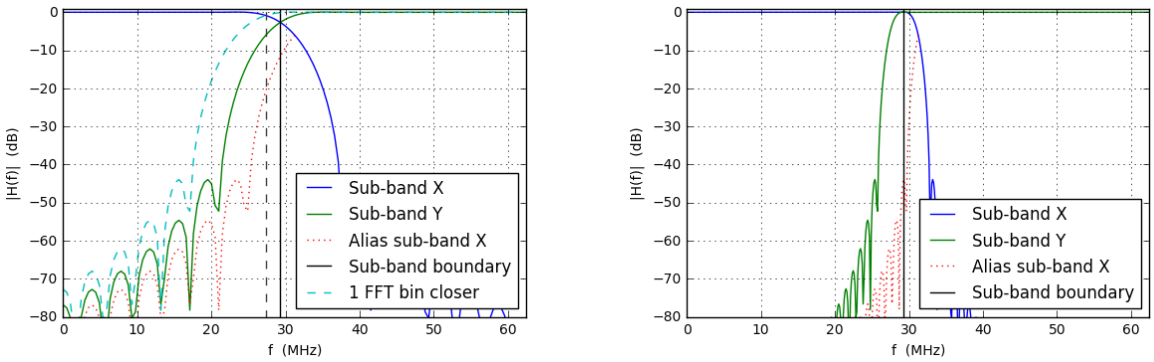

(a) 1024-point FFT *(b) 4-tap PFB*

Figure 7. An example of TFB channelization using 1024-point FFT and 32 sub-bands. (a) The sampling rate is 4 GHz. The dotted (red) line represents how Channel-X will alias over the Nyquist frequency after decimation. The dashed lines represent new Channel Y response and channel boundary when channel separation is made one FFT channel narrower. (b) The same example but using a 4-tap PFB with a 1024-point FFT.

the 1024[7] available sub-bands are selected to be sent to the correlator. In TDM, the FFT output is multiplied by the low-pass filter frequency response, and converted back to time domain through an Inverse FFT (IFFT), completing the overlap-save algorithm. Further optimization of the resource utilization can be achieved by shortening the length of this IFFT. This is possible when the sub-band tunability required for FDM imposes an FFT size which is bigger than what required by the design of the frequency converter low-pass filter. Then, a multi-resolution FFT [6] could be implemented at the first stage, so that different-length FFTs can be computed for FDM and TDM, while sharing resources.

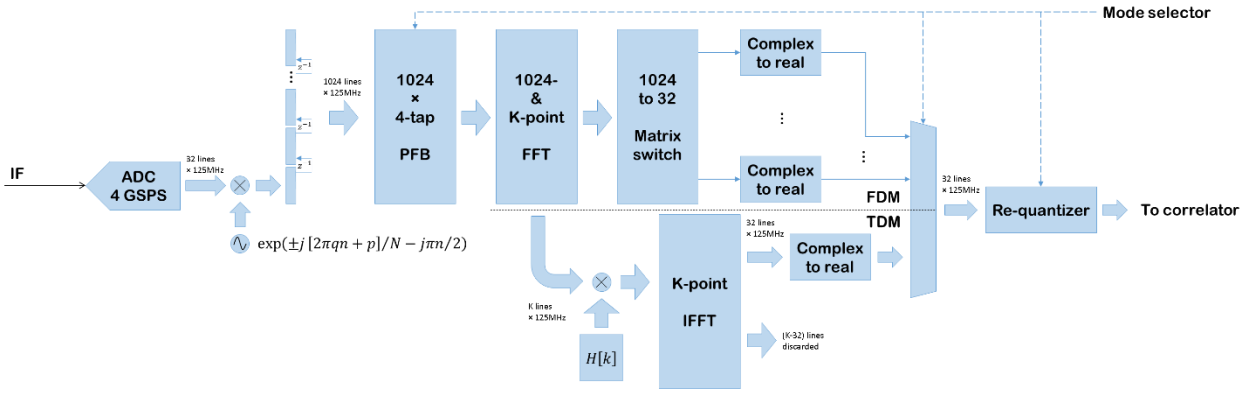

Figure 8. Simplified joint FDM-TDM architecture. A multi-resolution FFT allows efficient computation of K and 1024-point FFT [6].

[7] In practice, the set of FFT channels from which the 32 sub-bands are selected is reduced to less than 512 channels because only half the spectrum needs to be covered.

Conclusion

DIFS allows a great simplification of the analog backend by removing the second analog LO. However, the need for a second LO demands that it be implemented within the digital correlator. In FDM, the LO of the TFB can readily perform this task. On the contrary, TDM implementation needs to be modified accordingly. The new commonalities with FDM could be exploited for sharing resources while decreasing the new implementation cost. The new TDM implementation also enables finer delay tracking. However, the quantization efficiency degrades as compared to current TDM when the digital signal undergoes a frequency conversion, making it closer to the efficiency attained for FDM.

References

[1] S. Asayama, A. Biggs, I. de Gregorio, B. Dent, J. Di Francesco, E. Fomalont, A. Hales, J. Hibbard, G. Marconi, S. Kameno, B. Vila Vilaro, E. Villard and F. Stoehr, ALMA Cycle 5 Technical Handbook, ISBN 978-3-923524-66-2: ALMA Partnership, 2017.

[2] A. R. Thompson, J. M. Moran and G. W. Swenson Jr., Interferometry and Synthesis in Radio Astronomy, 3rd ed., Springer, 2017.

[3] A. R. Thompson, D. T. Emerson and F. R. Schwab, "Convenient formulas for quantization efficiency," *Radio Science*, vol. 42, 2007.

[4] A. Reilly, G. Frazer and B. Boashash, "Analytic signal generation-tips and traps," *IEEE Transactions on Signal Processing*, vol. 42, no. 11, pp. 3241-3245, 1994.

[5] A. Baudry et al., "Performance highlights of the ALMA correlators," in *Proc. SPIE 8452*, 2012.

[6] X. Wen and M. Sandler, "Calculation of radix-2 discrete multiresolution Fourier transform," *Signal Processing*, vol. 87, no. 10, pp. 2455-2460, 2007.

Acknowledgements

The authors would like to thank Fred Schwab for his comments and help while preparing this document.

Appendix A. Computation of the quantization efficiency

The quantization efficiency can be defined as the ratio of the sensitivity index with and without quantization. Consider again the simplified architecture in Figure 1, reproduced at the bottom of this page for convenience. The sensitivity index at the output of the correlator is:

$$d'_C = \frac{\mu_C}{\sigma_C} \tag{2}$$

where μ_C and σ_C are the mean and standard deviation of the correlator output. For interferometric measurements, μ_C becomes:

$$\mu_C = \mathrm{E}\left\{\sum_{n=0}^{N-1} y_1(n)\ y_2(n)\right\} = \sum_{n=0}^{N-1} \mathrm{E}\{y_1(n)\ y_2(n)\} \tag{3}$$

where the different subscripts mean both sequences are produced from different signals, arbitrarily labeled as 1 and 2. Perfect delay and fringe tracking is assumed. As regards σ_C ,

$$\sigma_C = \left[\mathrm{E}\left\{\left(\sum_{n=0}^{N-1} y_1(n)\ y_2(n)\right)^2\right\} - \mu_C^2\right]^{\frac{1}{2}} \tag{4}$$

$$= \left[\sum_{n,m=0}^{N-1} \mathrm{E}\{y_1(n)\ y_2(n)\ y_1(m)\ y_2(m)\} - \mu_C^2\right]^{\frac{1}{2}} \tag{5}$$

$$\simeq \left[\sum_{n,m=0}^{N-1} \mathrm{E}\{y_1(n)\ y_2(n)\}\ \mathrm{E}\{y_1(m)\ y_2(m)\} - \sum_{n=0}^{N-1} \mathrm{E}^2\{y_1(n)\ y_2(n)\} + \sum_{n=0}^{N} \mathrm{E}\{y_1^2(n)\ y_2^2(n)\} - \mu_C^2\right]^{\frac{1}{2}} \tag{6}$$

$$\simeq \left[\sum_{n=0}^{N-1} \mathrm{E}\{y_1^2(n)\ y_2^2(n)\} - \sum_{n=0}^{N-1} \mathrm{E}^2\{y_1(n)\ y_2(n)\}\right]^{\frac{1}{2}} \tag{7}$$

where the approximation is for flat spectrum (samples at different time are uncorrelated).

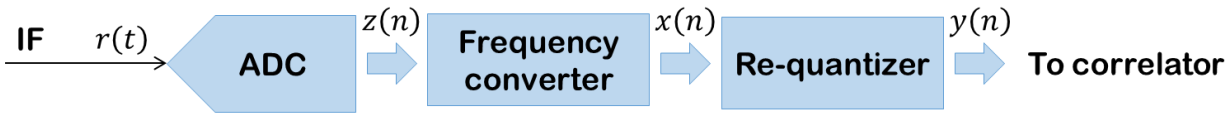

Figure 9. Simplified TDM architecture under study throughout this document

The sensitivity index for an ideal infinite precision ADC, where perfect delay and fringe tracking has been achieved prior to the ADC, would be:

$$d'_A = \frac{\mu_A}{\sigma_A} \tag{8}$$

where

$$\mu_A = \sum_{n=0}^{N-1} \mathrm{E}\{r_1(n)\ r_2(n)\} = N\ \mathrm{E}\{r_1(n)\ r_2(n)\} \tag{9}$$

and similarly to (7),

$$\sigma_A \simeq \sqrt{N}\ [\mathrm{E}\{r_1^2(n)\ r_2^2(n)\} - \mathrm{E}^2\{r_1(n)\ r_2(n)\}]^{\frac{1}{2}} \tag{10}$$

As result, the quantization efficiency is:

$$\eta_Q = \frac{d'_C}{d'_A} = \frac{\mu_C\ \sigma_A}{\sigma_C\ \mu_A} = \frac{\langle \mathrm{E}\{y_1(n)\ y_2(n)\}\rangle\ [\mathrm{E}\{r_1^2(n)\ r_2^2(n)\} - \mathrm{E}^2\{r_1(n)\ r_2(n)\}]^{\frac{1}{2}}}{\langle \mathrm{E}\{y_1^2(n)\ y_2^2(n)\} - \mathrm{E}^2\{y_1(n)\ y_2(n)\}\rangle^{\frac{1}{2}}\ \mathrm{E}\{r_1(n)\ r_2(n)\}} \tag{11}$$

where the angle brackets stand for the average over the correlator integration time. The quantization efficiency, as defined in (11), is in reality a function of the correlation between the two signals. As the efficiency is typically used for computing sensitivity, the asymptotic quantization efficiency for very small correlation is the only value of interest. Therefore,

$$\eta_Q = \lim_{\rho \to 0} \frac{\langle \mathrm{E}\{y_1(n)\ y_2(n)\}\rangle\ [\mathrm{E}\{r_1^2(n)\ r_2^2(n)\} - \mathrm{E}^2\{r_1(n)\ r_2(n)\}]^{\frac{1}{2}}}{\langle \mathrm{E}\{y_1^2(n)\ y_2^2(n)\} - \mathrm{E}^2\{y_1(n)\ y_2(n)\}\rangle^{\frac{1}{2}}\ \mathrm{E}\{r_1(n)\ r_2(n)\}} \tag{12}$$

where

$$\rho = \frac{\mathrm{E}\{r_1(n)\ r_2(n)\}}{[\mathrm{E}\{r_1^2(n)\}\ \mathrm{E}\{r_2^2(n)\}]^{\frac{1}{2}}} \tag{13}$$

is the Pearson correlation coefficient between the two signals (previous to quantization). In the limit, the two signals become independent, and thus

$$\begin{aligned} \lim_{\rho \to 0} \mathrm{E}\{r_1^2(n)\ r_2^2(n)\} - \mathrm{E}^2\{r_1(n)\ r_2(n)\} &= \mathrm{E}\{r_1^2(n)\}\ \mathrm{E}\{r_2^2(n)\} \\ \lim_{\rho \to 0} \mathrm{E}\{y_1^2(n)\ y_2^2(n)\} - \mathrm{E}^2\{y_1(n)\ y_2(n)\} &= \mathrm{E}\{y_1^2(n)\}\ \mathrm{E}\{y_2^2(n)\} \end{aligned} \tag{14}$$

which used in (12) yields:

$$\eta_Q = \langle \mathrm{E}\{y_1^2(n)\}\ \mathrm{E}\{y_2^2(n)\}\rangle^{-\frac{1}{2}}\ \lim_{\rho\to 0}\frac{\langle \mathrm{E}\{y_1(n)\ y_2(n)\}\rangle}{\rho} \tag{15}$$

Finally, L'Hôpital's rule guarantees that, if the limit exists, then:

$$\eta_Q = \langle \mathrm{E}\{y_1^2(n)\}\ \mathrm{E}\{y_2^2(n)\}\rangle^{-\frac{1}{2}}\ \langle \lim_{\rho\to 0}\frac{\partial}{\partial\rho}\mathrm{E}\{y_1(n)\ y_2(n)\}\rangle \tag{16}$$

which is the basis for the quantization efficiency computation within this appendix[8]. In order to compute η_Q, both the autocorrelation and the cross-correlation of $y(n)$ are needed.

A.1. Cross-correlation term

Let us focus first on the computation of $\langle \lim_{\rho\to 0}\frac{\partial}{\partial\rho}\mathrm{E}\{y_1(n)\ y_2(n)\}\rangle$. Assuming symmetry with respect to origin:

$$\mathrm{E}\{y_1(n)\ y_2(n)\} = 2\sum_{p,q=0}^{P-1}\left(p+\frac{1}{2}\right)\left(q+\frac{1}{2}\right)\left[\mathrm{P}_y^+(p,q;n) - \mathrm{P}_y^-(p,q;n)\right] \tag{17}$$

where $\mathrm{P}_y^+(q,p;n)$ is the probability that $y_1(n) = \left(p+\frac{1}{2}\right)$ and $y_2(n) = \left(q+\frac{1}{2}\right)$, while $\mathrm{P}_y^-(p,q;n)$ is the probability that $y_1(n) = \left(p+\frac{1}{2}\right)$ and $y_2(n) = -\left(q+\frac{1}{2}\right)$. Then,

$$\lim_{\rho\to 0}\frac{\partial}{\partial\rho}\mathrm{E}\{y_1(n)\ y_2(n)\} = 2\sum_{p,q=0}^{P-1}\left(p+\frac{1}{2}\right)\left(q+\frac{1}{2}\right)\left[\lim_{\rho\to 0}\frac{\partial}{\partial\rho}\mathrm{P}_y^+(p,q;n) - \lim_{\rho\to 0}\frac{\partial}{\partial\rho}\mathrm{P}_y^-(p,q;n)\right] \tag{18}$$

where P is half the number of quantization levels in the re-quantization process. The first quadrant probability is:

$$\mathrm{P}_y^+(p,q;n) = \int_{p\varepsilon}^{(p+1)\varepsilon}\int_{q\varepsilon}^{(q+1)\varepsilon} f_{xx}(x_1,x_2;n)\,dx_2\ dx_1 \tag{19}$$

where $f_{xx}(x_1,x_2;n)$ represents the joint PDF of $x_1(n)$ and $x_2(n)$, and ε is the re-quantization step. The upper limits in (19) extend to infinity for the last quantization level, viz. $p,q = P-1$. Similarly,

$$\mathrm{P}_y^-(p,q;n) = \int_{p\varepsilon}^{(p+1)\varepsilon}\int_{q\varepsilon}^{(q+1)\varepsilon} f_{xx}(x_1,-x_2;n)\,dx_2\ dx_1 \tag{20}$$

And taking the limit of the derivative results into:

$$\lim_{\rho\to 0}\frac{\partial}{\partial\rho}\mathrm{P}_y^+(p,q;n) = \int_{p\varepsilon}^{(p+1)\varepsilon}\int_{q\varepsilon}^{(q+1)\varepsilon}\lim_{\rho\to 0}\frac{\partial}{\partial\rho}f_{xx}(x_1,x_2;n)\ dx_2\ dx_1 \tag{21}$$

[8] As a sanity check, this expression can be used to obtain exactly the same results as in [3].

There is now the problem of determining the joint PDF $f_{xx}(x_1, x_2; n)$. This is what we know so far:

1) Both $x_1(n)$ and $x_2(n)$ follow the expression in (1):

$$x_i(n) = z_i(n)\ \cos(\omega_i n + \varphi_i) \mp \hat{z}_i(n)\ \sin(\omega_i n + \varphi_i) \tag{22}$$

where $z_i(n)$ is a discrete random variable and independent from $\hat{z}_i(n)$, which is Gaussian. However, in general, $z_1(n)$ and $\hat{z}_2(n)$ are not independent from each other; as well as neither are $\hat{z}_1(n)$ and $z_2(n)$ from each other.

2) If both signals $z_1(n)$ and $z_2(n)$ are converted using the same frequency and phase, i.e., $\omega = \omega_1 = \omega_2$ and $\varphi = \varphi_1 = \varphi_2$, then the cross-correlation is kept constant through the frequency converter:

$$\mathrm{E}\{x_1(n)\ x_2(n)\} = \mathrm{E}\{z_1(n)\ z_2(n)\} \tag{23}$$

As a result, $x_1(n)$ and $x_2(n)$ are jointly wide-sense stationary. This is straightforward from the frequency domain interpretation of the conversion process.

Most importantly, when the cosine term in (22) is zero, we get:

$$\mathrm{E}\{x_1(n)\ x_2(n)\} = \mathrm{E}\{\hat{z}_1(n)\ \hat{z}_2(n)\} = \mathrm{E}\{z_1(n)\ z_2(n)\} \tag{24}$$

which can be demonstrated to imply the independence of $z_1(n)$ and $\hat{z}_2(n)$ from each other, and hence, $\hat{z}_1(n)$ and $z_2(n)$ as well.

In this case, which the rest of the appendix focuses on, the joint PDF of $z_1(n)$, $z_2(n)$, $\hat{z}_1(n)$, and $\hat{z}_2(n)$ becomes:

$$f_{zz\hat{z}\hat{z}}(z_1, z_2, \hat{z}_1, \hat{z}_2) = f_{zz}(z_1, z_2)\ f_{\hat{z}\hat{z}}(\hat{z}_1, \hat{z}_2) \tag{25}$$

where[9]

$$\begin{aligned} f_{zz}(z_1, z_2) = &\sum_{l,m=0}^{M-1} \mathrm{P}_z^+(l, m)\ [\delta(z_1 - \tilde{z}_l)\ \delta(z_2 - \tilde{z}_m) + \delta(z_1 + \tilde{z}_l)\ \delta(z_2 + \tilde{z}_m)] \\ &+ \sum_{l,m=0}^{M-1} \mathrm{P}_z^-(l, m)\ [\delta(z_1 - \tilde{z}_l)\ \delta(z_2 + \tilde{z}_m) + \delta(z_1 + \tilde{z}_l)\ \delta(z_2 - \tilde{z}_m)] \end{aligned} \tag{26}$$

is the joint PDF of the ADC output, M is half the number of quantization levels, $\tilde{z}_k = k + \frac{1}{2}$ are the quantization values assigned to the ADC output,

$$\mathrm{P}_z^+(l, m) = \int_{l\Delta}^{(l+1)\Delta} \int_{m\Delta}^{(m+1)\Delta} f_{rr}(r_1, r_2)\ dr_2\ dr_1 \tag{27}$$

[9] Hereinafter, it is assumed for simplicity that both signals, $z_1(n)$ and $z_2(n)$, exhibit the same marginal statistics.

and

$$\mathrm{P}_z^-(l,m) = \int_{l\Delta}^{(l+1)\Delta} \int_{m\Delta}^{(m+1)\Delta} f_{rr}(r_1, -r_2)\, dr_2\ dr_1 \tag{28}$$

are the joint probabilities of $z_1(n)$ and $z_2(n)$, Δ is the ADC quantization step, and

$$f_{rr}(r_1, r_2) = \frac{1}{2\pi\sqrt{1-\rho^2}} \exp\left(\frac{2\rho\, r_1\, r_2 - r_1^2 - \hat{r}_2^2}{2(1-\rho^2)}\right) \tag{29}$$

assumes a jointly Gaussian ADC input and equal power. Additionally, in (25),

$$f_{\hat{z}\hat{z}}(\hat{z}_1, \hat{z}_2) = \frac{1}{2\pi\sigma_z^2\sqrt{1-\rho_z^2}} \exp\left(\frac{2\rho_z \hat{z}_1\, \hat{z}_2 - \hat{z}_1^2 - \hat{z}_2^2}{2\sigma_z^2(1-\rho_z^2)}\right) \tag{30}$$

where $\rho_z = \eta_A\, \rho$ is the correlation coefficient between $z_1(n)$ and $z_2(n)$, and η_A is the quantization efficiency of the ADC.

Once $f_{zz\hat{z}\hat{z}}(z_1, z_2, \hat{z}_1, \hat{z}_2)$ has been obtained, the joint PDF of $x_1(n)$ and $x_2(n)$ can be obtained through a multivariate transformation from (22). For simplicity, the joint PDF of the normalized variables $\tilde{x}_i(n) = \sigma_z^{-1}\, x_i(n)$ is developed instead. The only consequence is that the re-quantization step ε in (19)-(20) is now expressed in RMS units. Proceeding as indicated yields a bivariate Gaussian mixture for $\tilde{x}_1(n)$ and $\tilde{x}_2(n)$, where the weights are given by the joint probabilities of $z_1(n)$ and $z_2(n)$:

$$\begin{aligned} f_{\tilde{x}\tilde{x}}(\tilde{x}_1, \tilde{x}_2) = &\sum_{l,m=0}^{M-1} \mathrm{P}_z^+(l,m)\, [\Phi_2(\tilde{x}_1, \tilde{x}_2, \tilde{\mu}_l, \tilde{\mu}_m, \tilde{\sigma}_x, \rho_z; n) + \Phi_2(\tilde{x}_1, \tilde{x}_2, -\tilde{\mu}_l, -\tilde{\mu}_m, \tilde{\sigma}_x, \rho_z; n)] \\ &+ \sum_{l,m=0}^{M-1} \mathrm{P}_z^-(l,m)\, [\Phi_2(\tilde{x}_1, \tilde{x}_2, -\tilde{\mu}_l, \tilde{\mu}_m, \tilde{\sigma}_x, \rho_z; n) + \Phi_2(\tilde{x}_1, \tilde{x}_2, \tilde{\mu}_l, -\tilde{\mu}_m, \tilde{\sigma}_x, \rho_z; n)] \end{aligned} \tag{31}$$

where the parameters of each Gaussian in the mixture is a function of time:

$$\begin{aligned} &\Phi_2(\tilde{x}_1, \tilde{x}_2, \tilde{\mu}_l, \tilde{\mu}_m, \tilde{\sigma}_x, \rho_z; n) = \\ &= \frac{1}{2\pi\, \tilde{\sigma}_x^2(n)\, \sqrt{1-\rho_z^2}} \exp\left(\frac{2\rho_z[\tilde{x}_1 - \tilde{\mu}_l(n)][\tilde{x}_2 - \tilde{\mu}_m(n)] - [\tilde{x}_1 - \tilde{\mu}_l(n)]^2 - [\tilde{x}_2 - \tilde{\mu}_m(n)]^2}{2\, \tilde{\sigma}_x^2(n)\, (1-\rho_z^2)}\right) \end{aligned} \tag{32}$$

with

$$\tilde{\mu}_k(n) = \frac{\left(k + \frac{1}{2}\right)\cos(\omega n + \varphi)}{\sigma_z} \qquad \tilde{\sigma}_x^2(n) = \sin^2(\omega n + \varphi) \tag{33}$$

The Gaussian mixture degenerates to a discrete distribution:

$$f_{\tilde{x}\tilde{x}}(\tilde{x}_1, \tilde{x}_2) = f_{zz}(\sigma_z\, z_1, \sigma_z\, z_2) \tag{34}$$

when $\tilde{\sigma}_x^2(n) = 0$, and a bivariate Gaussian centered at the origin:

$$f_{\tilde{x}\tilde{x}}(\tilde{x}_1, \tilde{x}_2) = \sigma_z^2 \, f_{\hat{z}\hat{z}}(\sigma_z \, \hat{z}_1, \sigma_z \, \hat{z}_2) \tag{35}$$

when $\tilde{\sigma}_x^2(n) = 1$.

Therefore, the joint PDF of $\tilde{x}_1(n)$ and $\tilde{x}_2(n)$ consists of the sum of terms with the form:

$$\mathrm{P}_z^{\pm}(l, m) \;\; \Phi_2(\tilde{x}_1, \tilde{x}_2, \pm\tilde{\mu}_l, \pm\, \tilde{\mu}_m, \tilde{\sigma}_x, \rho_z; n) \tag{36}$$

These terms are to be differentiated and the limit taken in order to compute the efficiency. Then:

$$\begin{aligned} &\lim_{\rho \to 0} \frac{\partial}{\partial \rho} \mathrm{P}_z^{\pm}(l, m) \;\; \Phi_2(\tilde{x}_1, \tilde{x}_2, \pm\tilde{\mu}_l, \pm\, \tilde{\mu}_m, \tilde{\sigma}_x, \rho_z; n) \\ &\qquad = \Phi_2(\tilde{x}_1, \tilde{x}_2, \pm\tilde{\mu}_l, \pm\, \tilde{\mu}_m, \tilde{\sigma}_x, 0; n) \lim_{\rho \to 0} \frac{\partial}{\partial \rho} \mathrm{P}_z^{\pm}(l, m) \\ &\qquad + \lim_{\rho \to 0} \mathrm{P}_z^{\pm}(l, m) \;\; \lim_{\rho \to 0} \frac{\partial}{\partial \rho} \Phi_2(\tilde{x}_1, \tilde{x}_2, \pm\tilde{\mu}_l, \pm\, \tilde{\mu}_m, \tilde{\sigma}_x, \rho_z; n) \end{aligned} \tag{37}$$

Exploring each of these factors, it can be shown that:

$$\Phi_2(\tilde{x}_1, \tilde{x}_2, \pm\tilde{\mu}_l, \pm\, \tilde{\mu}_m, \tilde{\sigma}_x, 0; n) = \Phi_1(\tilde{x}_1, \pm\tilde{\mu}_l, \tilde{\sigma}_x; n) \;\; \Phi_1(\tilde{x}_2, \pm\tilde{\mu}_m, \tilde{\sigma}_x; n) \tag{38}$$

where

$$\Phi_1(x, \mu, \sigma; n) = \frac{1}{\sqrt{2\pi}\, \sigma(n)} \exp\left(- \left[\frac{x(n) - \mu(n)}{\sqrt{2}\, \sigma(n)} \right]^2 \right) \tag{39}$$

Additionally,

$$\lim_{\rho \to 0} \frac{\partial}{\partial \rho} \mathrm{P}_z^{\pm}(l, m) = \pm\, \dot{\mathrm{P}}_{\Delta}(l) \;\; \dot{\mathrm{P}}_{\Delta}(m) \tag{40}$$

where

$$\dot{\mathrm{P}}_{\Delta}(k) = \begin{cases} \dfrac{\exp\left(-\dfrac{[k\Delta]^2}{2} \right)}{\sqrt{2\pi}}, & k = M - 1 \\ \dfrac{\exp\left(-\dfrac{[k\Delta]^2}{2} \right) - \exp\left(-\dfrac{[(k+1)\Delta]^2}{2} \right)}{\sqrt{2\pi}}, & k = 0, \ldots, M - 2 \end{cases} \tag{41}$$

On the other hand,

$$\lim_{\rho \to 0} \mathrm{P}_z^{\pm}(l, m) = \mathrm{P}_{\Delta}(l) \;\; \mathrm{P}_{\Delta}(m)$$

where

$$\mathrm{P}_{\Delta}(k)=\begin{cases}\dfrac{1-\operatorname{erf}\left(\dfrac{k\Delta}{\sqrt{2}}\right)}{2}, & k=M-1\\ \dfrac{\operatorname{erf}\left(\dfrac{(k+1)\Delta}{\sqrt{2}}\right)-\operatorname{erf}\left(\dfrac{k\Delta}{\sqrt{2}}\right)}{2}, & k=0,\dots,M-2\end{cases} \tag{42}$$

And finally,

$$\begin{aligned}\lim_{\rho\to 0}\frac{\partial}{\partial\rho}\Phi_2(\tilde{x}_1,\tilde{x}_2,\pm\tilde{\mu}_l,\pm\tilde{\mu}_m,\tilde{\sigma}_x,\rho_z;n) &= \eta_A\lim_{\rho_z\to 0}\frac{\partial}{\partial\rho_z}\Phi_2(\tilde{x}_1,\tilde{x}_2,\pm\tilde{\mu}_l,\pm\tilde{\mu}_m,\tilde{\sigma}_x,\rho_z;n)\\ &= \eta_A\ \Phi_1(\tilde{x}_1,\pm\tilde{\mu}_l,\tilde{\sigma}_x;n)\ \Phi_1(\tilde{x}_2,\pm\tilde{\mu}_m,\tilde{\sigma}_x;n)\frac{[\tilde{x}_1\mp\tilde{\mu}_l(n)][\tilde{x}_2\mp\tilde{\mu}_m(n)]}{\tilde{\sigma}_x^2(n)}\end{aligned} \tag{43}$$

Using all the previous results into (21), with the re-quantization step in RMS units in order to account for the normalization, namely $\tilde{\varepsilon}=\varepsilon/\sigma_z$, yields:

$$\lim_{\rho\to 0}\frac{\partial}{\partial\rho}\mathrm{P}_y^{+}(p,q;n)=\int_{p\tilde{\varepsilon}}^{(p+1)\tilde{\varepsilon}}\int_{q\tilde{\varepsilon}}^{(q+1)\tilde{\varepsilon}}\lim_{\rho\to 0}\frac{\partial}{\partial\rho}f_{\tilde{x}\tilde{x}}(\tilde{x}_1,\tilde{x}_2;n)\ d\tilde{x}_2\ d\tilde{x}_1 \tag{44}$$

$$\begin{aligned}&=\sum_{l,m=0}^{M-1}\int_{p\tilde{\varepsilon}}^{(p+1)\tilde{\varepsilon}}\int_{q\tilde{\varepsilon}}^{(q+1)\tilde{\varepsilon}}\lim_{\rho\to 0}\frac{\partial}{\partial\rho}\mathrm{P}_z^{+}(l,m)\,[\Phi_2(\tilde{x}_1,\tilde{x}_2,\tilde{\mu}_l,\tilde{\mu}_m,\tilde{\sigma}_x,\rho_z;n)\\ &\qquad+\Phi_2(\tilde{x}_1,\tilde{x}_2,-\tilde{\mu}_l,-\tilde{\mu}_m,\tilde{\sigma}_x,\rho_z;n)]\,d\tilde{x}_2\ d\tilde{x}_1\\ &+\sum_{l,m=0}^{M-1}\int_{p\tilde{\varepsilon}}^{(p+1)\tilde{\varepsilon}}\int_{q\tilde{\varepsilon}}^{(q+1)\tilde{\varepsilon}}\lim_{\rho\to 0}\frac{\partial}{\partial\rho}\mathrm{P}_z^{-}(l,m)\,[\Phi_2(\tilde{x}_1,\tilde{x}_2,-\tilde{\mu}_l,\tilde{\mu}_m,\tilde{\sigma}_x,\rho_z;n)\\ &\qquad+\Phi_2(\tilde{x}_1,\tilde{x}_2,\tilde{\mu}_l,-\tilde{\mu}_m,\tilde{\sigma}_x,\rho_z;n)]\,d\tilde{x}_2\ d\tilde{x}_1\end{aligned} \tag{45}$$

$$
\begin{aligned}
&= \sum_{l=0}^{M-1} \dot{\mathrm{P}}_{\Delta}(l) \int_{p\tilde{\varepsilon}}^{(p+1)\tilde{\varepsilon}} \Phi_1(\tilde{x}_1, \tilde{\mu}_l, \tilde{\sigma}_x; n)\, d\tilde{x}_1 \sum_{m=0}^{M-1} \dot{\mathrm{P}}_{\Delta}(m) \int_{q\tilde{\varepsilon}}^{(q+1)\tilde{\varepsilon}} \Phi_1(\tilde{x}_2, \tilde{\mu}_m, \tilde{\sigma}_x; n)\, d\tilde{x}_2 \\
&+ \frac{\eta_A}{\tilde{\sigma}_x^2(n)} \sum_{l=0}^{M-1} \mathrm{P}_{\Delta}(l) \int_{p\tilde{\varepsilon}}^{(p+1)\tilde{\varepsilon}} \Phi_1(\tilde{x}_1, \tilde{\mu}_l, \tilde{\sigma}_x; n)\, [\tilde{x}_1 - \tilde{\mu}_l(n)] d\tilde{x}_1 \\
&\qquad \times \sum_{m=0}^{M-1} \mathrm{P}_{\Delta}(m) \int_{q\tilde{\varepsilon}}^{(q+1)\tilde{\varepsilon}} \Phi_1(\tilde{x}_2, \tilde{\mu}_m, \tilde{\sigma}_x; n)\, [\tilde{x}_2 - \tilde{\mu}_m(n)] d\tilde{x}_2 \\
&+ \sum_{l=0}^{M-1} \dot{\mathrm{P}}_{\Delta}(l) \int_{p\tilde{\varepsilon}}^{(p+1)\tilde{\varepsilon}} \Phi_1(\tilde{x}_1, -\tilde{\mu}_l, \tilde{\sigma}_x; n)\, d\tilde{x}_1 \sum_{m=0}^{M-1} \dot{\mathrm{P}}_{\Delta}(m) \int_{q\tilde{\varepsilon}}^{(q+1)\tilde{\varepsilon}} \Phi_1(\tilde{x}_2, -\tilde{\mu}_m, \tilde{\sigma}_x; n)\, d\tilde{x}_2 \\
&+ \frac{\eta_A}{\tilde{\sigma}_x^2(n)} \sum_{l=0}^{M-1} \mathrm{P}_{\Delta}(l) \int_{p\tilde{\varepsilon}}^{(p+1)\tilde{\varepsilon}} \Phi_1(\tilde{x}_1, -\tilde{\mu}_l, \tilde{\sigma}_x; n)\, [\tilde{x}_1 + \tilde{\mu}_l(n)] d\tilde{x}_1 \\
&\qquad \times \sum_{m=0}^{M-1} \mathrm{P}_{\Delta}(m) \int_{q\tilde{\varepsilon}}^{(q+1)\tilde{\varepsilon}} \Phi_1(\tilde{x}_2, -\tilde{\mu}_m, \tilde{\sigma}_x; n)\, [\tilde{x}_2 + \tilde{\mu}_m(n)] d\tilde{x}_2 \\
&- \sum_{l=0}^{M-1} \dot{\mathrm{P}}_{\Delta}(l) \int_{p\tilde{\varepsilon}}^{(p+1)\tilde{\varepsilon}} \Phi_1(\tilde{x}_1, -\tilde{\mu}_l, \tilde{\sigma}_x; n)\, d\tilde{x}_1 \sum_{m=0}^{M-1} \dot{\mathrm{P}}_{\Delta}(m) \int_{q\tilde{\varepsilon}}^{(q+1)\tilde{\varepsilon}} \Phi_1(\tilde{x}_2, \tilde{\mu}_m, \tilde{\sigma}_x; n)\, d\tilde{x}_2 \\
&+ \frac{\eta_A}{\tilde{\sigma}_x^2(n)} \sum_{l=0}^{M-1} \mathrm{P}_{\Delta}(l) \int_{p\tilde{\varepsilon}}^{(p+1)\tilde{\varepsilon}} \Phi_1(\tilde{x}_1, -\tilde{\mu}_l, \tilde{\sigma}_x; n)\, [\tilde{x}_1 + \tilde{\mu}_l(n)] d\tilde{x}_1 \\
&\qquad \times \sum_{m=0}^{M-1} \mathrm{P}_{\Delta}(m) \int_{q\tilde{\varepsilon}}^{(q+1)\tilde{\varepsilon}} \Phi_1(\tilde{x}_2, \tilde{\mu}_m, \tilde{\sigma}_x; n)\, [\tilde{x}_2 - \tilde{\mu}_m(n)] d\tilde{x}_2 \\
&- \sum_{l=0}^{M-1} \dot{\mathrm{P}}_{\Delta}(l) \int_{p\tilde{\varepsilon}}^{(p+1)\tilde{\varepsilon}} \Phi_1(\tilde{x}_1, \tilde{\mu}_l, \tilde{\sigma}_x; n)\, d\tilde{x}_1 \sum_{m=0}^{M-1} \dot{\mathrm{P}}_{\Delta}(m) \int_{q\tilde{\varepsilon}}^{(q+1)\tilde{\varepsilon}} \Phi_1(\tilde{x}_2, -\tilde{\mu}_m, \tilde{\sigma}_x; n)\, d\tilde{x}_2 \\
&+ \frac{\eta_A}{\tilde{\sigma}_x^2(n)} \sum_{l=0}^{M-1} \mathrm{P}_{\Delta}(l) \int_{p\tilde{\varepsilon}}^{(p+1)\tilde{\varepsilon}} \Phi_1(\tilde{x}_1, \tilde{\mu}_l, \tilde{\sigma}_x; n)\, [\tilde{x}_1 - \tilde{\mu}_l(n)] d\tilde{x}_1 \\
&\qquad \times \sum_{m=0}^{M-1} \mathrm{P}_{\Delta}(m) \int_{q\tilde{\varepsilon}}^{(q+1)\tilde{\varepsilon}} \Phi_1(\tilde{x}_2, -\tilde{\mu}_m, \tilde{\sigma}_x; n)\, [\tilde{x}_2 + \tilde{\mu}_m(n)] d\tilde{x}_2
\end{aligned}
\tag{46}
$$

Rearranging terms:

$$\lim_{\rho\to 0}\frac{\partial}{\partial\rho}\mathrm{P}_y^{+}(p,q;n)=\sum_{l=0}^{M-1}\dot{\mathrm{P}}_{\Delta}(l)\int_{p\tilde{\varepsilon}}^{(p+1)\tilde{\varepsilon}}[\Phi_1(\tilde{x}_1,\tilde{\mu}_l,\tilde{\sigma}_x;n)-\Phi_1(\tilde{x}_1,-\tilde{\mu}_l,\tilde{\sigma}_x;n)]d\tilde{x}_1$$
$$\times\sum_{m=0}^{M-1}\dot{\mathrm{P}}_{\Delta}(m)\int_{q\tilde{\varepsilon}}^{(q+1)\tilde{\varepsilon}}[\Phi_1(\tilde{x}_2,\tilde{\mu}_m,\tilde{\sigma}_x;n)-\Phi_1(\tilde{x}_2,-\tilde{\mu}_m,\tilde{\sigma}_x;n)]d\tilde{x}_2$$
$$+\frac{\eta_A}{\tilde{\sigma}_x^2(n)}\sum_{l=0}^{M-1}\mathrm{P}_{\Delta}(l)\int_{p\tilde{\varepsilon}}^{(p+1)\tilde{\varepsilon}}(\Phi_1(\tilde{x}_1,\tilde{\mu}_l,\tilde{\sigma}_x;n)\,[\tilde{x}_1-\tilde{\mu}_l(n)]+\Phi_1(\tilde{x}_1,-\tilde{\mu}_l,\tilde{\sigma}_x;n)\,[\tilde{x}_1+\tilde{\mu}_l(n)])d\tilde{x}_1$$
$$\times\sum_{m=0}^{M-1}\mathrm{P}_{\Delta}(m)\int_{q\tilde{\varepsilon}}^{(q+1)\tilde{\varepsilon}}(\Phi_1(\tilde{x}_2,\tilde{\mu}_m,\tilde{\sigma}_x;n)\,[\tilde{x}_2-\tilde{\mu}_m(n)]+\Phi_1(\tilde{x}_2,-\tilde{\mu}_m,\tilde{\sigma}_x;n)\,[\tilde{x}_2+\tilde{\mu}_m(n)])d\tilde{x}_2 \tag{47}$$

Similarly,

$$\lim_{\rho\to 0}\frac{\partial}{\partial\rho}\mathrm{P}_y^{-}(p,q;n)=\sum_{l=0}^{M-1}\dot{\mathrm{P}}_{\Delta}(l)\int_{p\tilde{\varepsilon}}^{(p+1)\tilde{\varepsilon}}[\Phi_1(\tilde{x}_1,\tilde{\mu}_l,\tilde{\sigma}_x;n)-\Phi_1(\tilde{x}_1,-\tilde{\mu}_l,\tilde{\sigma}_x;n)]d\tilde{x}_1$$
$$\times\sum_{m=0}^{M-1}\dot{\mathrm{P}}_{\Delta}(m)\int_{q\tilde{\varepsilon}}^{(q+1)\tilde{\varepsilon}}[\Phi_1(\tilde{x}_2,-\tilde{\mu}_m,\tilde{\sigma}_x;n)-\Phi_1(\tilde{x}_2,\tilde{\mu}_m,\tilde{\sigma}_x;n)]d\tilde{x}_2$$
$$-\frac{\eta_A}{\tilde{\sigma}_x^2(n)}\sum_{l=0}^{M-1}\mathrm{P}_{\Delta}(l)\int_{p\tilde{\varepsilon}}^{(p+1)\tilde{\varepsilon}}(\Phi_1(\tilde{x}_1,\tilde{\mu}_l,\tilde{\sigma}_x;n)\,[\tilde{x}_1-\tilde{\mu}_l(n)]+\Phi_1(\tilde{x}_1,-\tilde{\mu}_l,\tilde{\sigma}_x;n)\,[\tilde{x}_1+\tilde{\mu}_l(n)])d\tilde{x}_1$$
$$\times\sum_{m=0}^{M-1}\mathrm{P}_{\Delta}(m)\int_{q\tilde{\varepsilon}}^{(q+1)\tilde{\varepsilon}}(\Phi_1(\tilde{x}_2,-\tilde{\mu}_m,\tilde{\sigma}_x;n)\,[\tilde{x}_2+\tilde{\mu}_m(n)]+\Phi_1(\tilde{x}_2,\tilde{\mu}_m,\tilde{\sigma}_x;n)\,[\tilde{x}_2-\tilde{\mu}_m(n)])d\tilde{x}_2 \tag{48}$$

where the identity

$$\Phi_1(-x,\mu,\sigma;n)=\Phi_1(x,-\mu,\sigma;n) \tag{49}$$

has been used. As a result, the subtraction in the right-hand side term of (18) becomes:

$$\lim_{\rho\to 0}\frac{\partial}{\partial\rho}\mathrm{P}_y^{+}(p,q;n)-\lim_{\rho\to 0}\frac{\partial}{\partial\rho}\mathrm{P}_y^{-}(p,q;n)=2\lim_{\rho\to 0}\frac{\partial}{\partial\rho}\mathrm{P}_y^{+}(p,q;n) \tag{50}$$

Therefore, the cross-correlation term of the quantization efficiency in (16) that we are looking for results:

$$\left\langle \lim_{\rho\to 0}\frac{\partial}{\partial\rho}\mathrm{E}\{y_1(n)\ y_2(n)\}\right\rangle = \left\langle \left[\sum_{p=0}^{P-1}\left(p+\frac{1}{2}\right)\sum_{l=0}^{M-1}\dot{\mathrm{P}}_{\Delta}(l)\ \mathrm{P}_{\varepsilon}(p,l;n)\right]^2\right\rangle + \eta_A\left\langle \left[\sum_{p=0}^{P-1}\left(p+\frac{1}{2}\right)\sum_{l=0}^{M-1}\mathrm{P}_{\Delta}(l)\ \dot{\mathrm{P}}_{\varepsilon}(p,l;n)\right]^2\right\rangle \tag{51}$$

where[10,11]

$$\mathrm{P}_{\varepsilon}(p,l;n) = 2\int_{p\tilde{\varepsilon}}^{(p+1)\tilde{\varepsilon}}[\Phi_1(\tilde{x},\tilde{\mu}_l,\tilde{\sigma}_x;n)-\Phi_1(\tilde{x},-\tilde{\mu}_l,\tilde{\sigma}_x;n)]d\tilde{x}$$

$$= \begin{cases} \mathrm{erf}\left(\dfrac{(p+1)\,\varepsilon-\left(l+\frac{1}{2}\right)\cos(\omega n+\varphi)}{\sqrt{2}\,\sigma_z|\sin(\omega n+\varphi)|}\right) \\ -\mathrm{erf}\left(\dfrac{p\,\varepsilon-\left(l+\frac{1}{2}\right)\cos(\omega n+\varphi)}{\sqrt{2}\,\sigma_z|\sin(\omega n+\varphi)|}\right) \\ -\mathrm{erf}\left(\dfrac{(p+1)\,\varepsilon+\left(l+\frac{1}{2}\right)\cos(\omega n+\varphi)}{\sqrt{2}\,\sigma_z|\sin(\omega n+\varphi)|}\right) \\ +\mathrm{erf}\left(\dfrac{p\,\varepsilon+\left(l+\frac{1}{2}\right)\cos(\omega n+\varphi)}{\sqrt{2}\,\sigma_z|\sin(\omega n+\varphi)|}\right) \end{cases} \quad p=0,\dots,P-2$$

$$= \begin{cases} \mathrm{erf}\left(\dfrac{p\,\varepsilon+\left(l+\frac{1}{2}\right)\cos(\omega n+\varphi)}{\sqrt{2}\,\sigma_z|\sin(\omega n+\varphi)|}\right) \\ -\mathrm{erf}\left(\dfrac{p\,\varepsilon-\left(l+\frac{1}{2}\right)\cos(\omega n+\varphi)}{\sqrt{2}\,\sigma_z|\sin(\omega n+\varphi)|}\right) \end{cases} \quad p=P-1 \tag{52}$$

[10] The license taken by using $(p+1)\tilde{\varepsilon}$ as the upper limit of the integral at $p=P-1$ is corrected here.

[11] Both (52) and (53) require dividing by zero at some instants. The result can be interpreted as infinite with the same sign as the numerator. Both the Gaussian and the error functions yield finite values for infinite arguments, so this should not be a problem for the computation of the efficiency. However, the quotient is not defined if the numerator is zero too. This occurs when any output value of the ADC falls at the edge between two re-quantization levels. This situation can be avoided through careful selection of the re-quantization step.

and

$$\dot{\mathrm{P}}_{\varepsilon}(p,l;n)=\frac{2}{\tilde{\sigma}_x}\int_{p\tilde{\varepsilon}}^{(p+1)\tilde{\varepsilon}}\left(\Phi_1(\tilde{x},\tilde{\mu}_l,\tilde{\sigma}_x;n)\,[\tilde{x}-\tilde{\mu}_l(n)]+\Phi_1(\tilde{x},-\tilde{\mu}_l,\tilde{\sigma}_x;n)\,[\tilde{x}+\tilde{\mu}_l(n)]\right)d\tilde{x}$$

$$=\sqrt{\frac{2}{\pi}}\times\begin{cases}-\exp\left(-\left[\dfrac{(p+1)\,\varepsilon-\left(l+\frac{1}{2}\right)\cos(\omega n+\varphi)}{\sqrt{2}\,\sigma_z|\sin(\omega n+\varphi)|}\right]^2\right)\\ +\exp\left(-\left[\dfrac{p\,\varepsilon-\left(l+\frac{1}{2}\right)\cos(\omega n+\varphi)}{\sqrt{2}\,\sigma_z|\sin(\omega n+\varphi)|}\right]^2\right)\\ -\exp\left(-\left[\dfrac{(p+1)\,\varepsilon+\left(l+\frac{1}{2}\right)\cos(\omega n+\varphi)}{\sqrt{2}\,\sigma_z|\sin(\omega n+\varphi)|}\right]^2\right)\\ +\exp\left(-\left[\dfrac{p\,\varepsilon+\left(l+\frac{1}{2}\right)\cos(\omega n+\varphi)}{\sqrt{2}\,\sigma_z|\sin(\omega n+\varphi)|}\right]^2\right)\end{cases}\quad p=0,\dots,P-2$$

$$\begin{cases}\exp\left(-\left[\dfrac{p\,\varepsilon-\left(l+\frac{1}{2}\right)\cos(\omega n+\varphi)}{\sqrt{2}\,\sigma_z|\sin(\omega n+\varphi)|}\right]^2\right)\\ +\exp\left(-\left[\dfrac{p\,\varepsilon+\left(l+\frac{1}{2}\right)\cos(\omega n+\varphi)}{\sqrt{2}\,\sigma_z|\sin(\omega n+\varphi)|}\right]^2\right)\end{cases}\quad p=P-1 \tag{53}$$

Although cumbersome, the above expressions can be evaluated with the help of a computer in less one second per (Δ,ε) pair. Finally, for the sake of completeness, the standard deviation of the ADC output can be computed as:

$$\sigma_z=\sum_{p=0}^{P-1}\left(p+\frac{1}{2}\right)^2\mathrm{P}_{\Delta}(p) \tag{54}$$

A.2. Auto-correlation terms

The result of the previous section has to be multiplied by the re-quantizer output variance in order to obtain the overall quantization efficiency, see (16). As the variance can be marginally computed, the signal label subscript will be dropped in the following:

$$\mathrm{E}\{y^2(n)\} = 2\sum_{p=0}^{P-1}\left(p+\frac{1}{2}\right)^2 \mathrm{P}_y(p;n) \tag{55}$$

where[12]

$$\mathrm{P}_y(p;n) = \int_{p\varepsilon}^{(p+1)\varepsilon} f_x(x;n)\,dx \tag{56}$$

is the probability that $y(n) = \left(p+\frac{1}{2}\right)$, and $f_x(x;n)$ is the PDF of $x(n)$. From (1), and given that $z(n)$ and its Hilbert transform are independent from each other, then $f_x(x)$ results from the convolution:

$$f_x(x;n) = f_{zc}(x;n) \circledast f_{\hat{z}s}(x;n) \tag{57}$$

where

$$f_{zc}(x;n) = \sum_{m=0}^{M-1} \mathrm{P}_\Delta(m)\left(\delta\left[x(n) - \left(m+\frac{1}{2}\right)\cos(\omega n+\varphi)\right] + \delta\left[x(n) + \left(m+\frac{1}{2}\right)\cos(\omega n+\varphi)\right]\right) \tag{58}$$

is the PDF of $z(n)\cos(\omega n+\varphi)$ and

$$f_{\hat{z}s}(x;n) = \frac{1}{\sqrt{2\pi}\sigma_z|\sin(\omega n+\varphi)|}\exp\left(-\left[\frac{x(n)}{\sqrt{2}\sigma_z|\sin(\omega n+\varphi)|}\right]^2\right) \tag{59}$$

is the PDF of $\hat{z}(n)\sin(\omega n+\varphi)$. As a result, $f_x(x;n)$ follows a Gaussian mixture model:

$$f_x(x;n) = \sum_{m=0}^{M-1} \mathrm{P}_\Delta(m)\left[\Phi_1(x,\mu_m,\sigma_{\hat{z}s};n) + \Phi_1(x,-\mu_m,\sigma_{\hat{z}s};n)\right] \tag{60}$$

where:

$$\mu_m(n) = \left(m+\frac{1}{2}\right)\cos(\omega n+\varphi) \qquad\qquad \sigma_{\hat{z}s}(n) = \sigma_z|\sin(\omega n+\varphi)| \tag{61}$$

Using these results in (55) yields:

$$\mathrm{E}\{y^2(n)\} = 2\sum_{q=0}^{P-1}\left(q+\frac{1}{2}\right)^2 \sum_{m=0}^{M-1} \mathrm{P}_\Delta(m)\int_{q\varepsilon}^{(q+1)\varepsilon}\left[\Phi_1(x,\mu_m,\sigma_{\hat{z}s};n) + \Phi_1(x,-\mu_m,\sigma_{\hat{z}s};n)\right]dx \tag{62}$$

which, after considering the infinite upper limit at $q = P-1$, becomes:

[12] Again, the upper limit of the integral must extend to infinity for the last quantization level.

$$\mathrm{E}\{y^2(n)\} = \sum_{q=0}^{P-2}\left(q+\frac{1}{2}\right)^2 \sum_{m=0}^{M-1} \mathrm{P}_\Delta(m)\left[\mathrm{erf}\left(\frac{(q+1)\,\varepsilon-\mu_m(n)}{\sqrt{2}\;\sigma_{\hat{z}s}(n)}\right)-\mathrm{erf}\left(\frac{q\,\varepsilon-\mu_m(n)}{\sqrt{2}\;\sigma_{\hat{z}s}(n)}\right)\right.$$
$$\left.+\,\mathrm{erf}\left(\frac{(q+1)\,\varepsilon+\mu_m(n)}{\sqrt{2}\;\sigma_{\hat{z}s}(n)}\right)-\mathrm{erf}\left(\frac{q\,\varepsilon+\mu_m(n)}{\sqrt{2}\;\sigma_{\hat{z}s}(n)}\right)\right] \qquad (63)$$
$$+\left(P-\frac{1}{2}\right)^2 \sum_{m=0}^{M-1} \mathrm{P}_\Delta(m)\left[2-\mathrm{erf}\left(\frac{q\,\varepsilon-\mu_m(n)}{\sqrt{2}\;\sigma_{\hat{z}s}(n)}\right)-\mathrm{erf}\left(\frac{q\,\varepsilon+\mu_m(n)}{\sqrt{2}\;\sigma_{\hat{z}s}(n)}\right)\right]$$

Rearranging terms, the expression can be simplified as:

$$\mathrm{E}\{y^2(n)\} = \left(P-\frac{1}{2}\right)^2 - 2\sum_{m=0}^{M-1}\sum_{q=1}^{P-1} \mathrm{P}_\Delta(m)\,q\left[\mathrm{erf}\left(\frac{q\,\varepsilon-\mu_m(n)}{\sqrt{2}\;\sigma_{\hat{z}s}(n)}\right)+\mathrm{erf}\left(\frac{q\,\varepsilon+\mu_m(n)}{\sqrt{2}\;\sigma_{\hat{z}s}(n)}\right)\right] \qquad (64)$$

Taking the RMS value of this result over time and multiplying by the cross-correlation term obtained in the previous section, produces the desired overall quantization efficiency, see (16).

Appendix B. Approximate quantization efficiency

The results in Appendix A are valid only when the same phase and frequency is used at the frequency converters for both signals. In this appendix, we follow a more general approach based on [3], which unfortunately, attains less accuracy in the computation of the quantization efficiency when the quantizer input is non-Gaussian.

From the definition of quantization efficiency, it is straightforward that the overall efficiency is the product of the efficiencies of the ADC and the re-quantizer. Whereas the ADC efficiency is well-known, only the re-quantizer's efficiency is of interest.

By the approach in [3], the re-quantizer output $y(n)$ is expressed as a scaled version of the input minus a quantization error:

$$y(n) = a(n)\,[x(n) - q(n)] \tag{65}$$

or equivalently,

$$x(n) = \alpha(n)\,y(n) + q(n) \tag{66}$$

where the scale is set such that the quantization error and the input are orthogonal:

$$\alpha(n) = a^{-1}(n) = \frac{\mathrm{E}\{x^2(n)\}}{\mathrm{E}\{x(n)\,y(n)\}} \tag{67}$$

On the other hand, the quantization efficiency can be defined as the ratio of the sensitivity index with and without quantization. Consider again the simplified architecture in Figure 1, reproduced at the bottom of this page for convenience. The sensitivity index at the output of the correlator is:

$$d_C' = \frac{\mu_C}{\sigma_C} \tag{68}$$

where μ_C and σ_C are the mean and standard deviation of the correlator output. For interferometric measurements, μ_C becomes:

$$\mu_C = \mathrm{E}\left\{\sum_{n=0}^{N-1} y_1(n)\ y_2(n)\right\} = \sum_{n=0}^{N-1} \mathrm{E}\{y_1(n)\ y_2(n)\} \tag{69}$$

Using (65), we obtain:

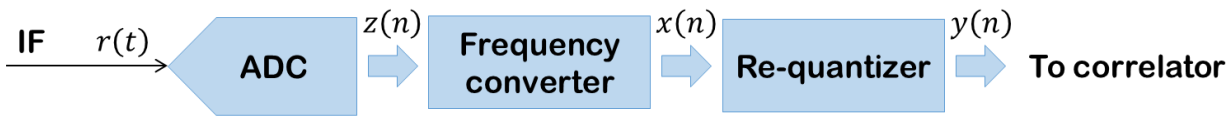

Figure 10. Simplified TDM architecture under study throughout this document

$$\mu_C = \sum_{n=0}^{N-1} a_1(n)\, a_2(n)\, \mathrm{E}\{[x_1(n) - q_1(n)][x_2(n) - q_2(n)]\} \tag{70}$$

The lack of accuracy of this approach arises from approximating the above equation as:

$$\mu_C \simeq \sum_{n=0}^{N-1} a_1(n)\, a_2(n)\, \mathrm{E}\{x_1(n)\, x_2(n)\} = \mathrm{E}\{x_1(n)\, x_2(n)\} \sum_{n=0}^{N-1} a_1(n)\, a_2(n) \tag{71}$$

under the assumption that the quantization noise for one signal is little or non-correlated with the other signal and vice versa. This assumption has been proved to be accurate for Gaussian inputs, e.g., in ADCs, but as shall be shown, it incurs a slight error for the Gaussian mixture distribution of $x(n)$.

As shown in Appendix A, when the input spectrum is flat and the correlation coefficient is small,

$$\sigma_C \simeq \left[\sum_{n=0}^{N-1} \mathrm{E}\{y_1^2(n)\}\ \mathrm{E}\{y_2^2(n)\}\right]^{\frac{1}{2}} \tag{72}$$

and similarly for the non-quantized input,

$$\mu_{Cx} \simeq \sum_{n=0}^{N-1} \mathrm{E}\{x_1(n)\, x_2(n)\} = N\, \mathrm{E}\{x_1(n)\, x_2(n)\} \tag{73}$$

and

$$\sigma_{Cx} \simeq \left[\sum_{n=0}^{N-1} \mathrm{E}\{x_1^2(n)\}\ \mathrm{E}\{x_2^2(n)\}\right]^{\frac{1}{2}} = [N\, \mathrm{E}\{x_1^2(n)\}\ \mathrm{E}\{x_2^2(n)\}]^{\frac{1}{2}} \tag{74}$$

Therefore, assuming equal statistics for both signals, $\mathrm{E}\{x_1^2(n)\} = \mathrm{E}\{x_2^2(n)\} = \mathrm{E}\{x^2(n)\}$. The re-quantizer's efficiency for small correlation coefficient results in:

$$\eta_Q = \frac{\mu_C\, \sigma_{Cx}}{\sigma_C\, \mu_{Cx}} \simeq \frac{\langle a_1(n)\, a_2(n)\rangle\, \mathrm{E}\{x^2(n)\}}{\langle \mathrm{E}\{y_1^2(n)\}\ \mathrm{E}\{y_2^2(n)\}\rangle^{\frac{1}{2}}} \tag{75}$$

using (67) yields:

$$\eta_Q \simeq \frac{\langle \frac{\mathrm{E}\{x_1(n)\, y_1(n)\}\, \mathrm{E}\{x_2(n)\, y_2(n)\}}{\mathrm{E}^2\{x^2(n)\}} \rangle\, \mathrm{E}\{x^2(n)\}}{\langle \mathrm{E}\{y_1^2(n)\}\ \mathrm{E}\{y_2^2(n)\}\rangle^{\frac{1}{2}}} = \frac{\langle \mathrm{E}\{x_1(n)\, y_1(n)\}\, \mathrm{E}\{x_2(n)\, y_2(n)\}\rangle}{\mathrm{E}\{x^2(n)\}\ \langle \mathrm{E}\{y_1^2(n)\}\ \mathrm{E}\{y_2^2(n)\}\rangle^{\frac{1}{2}}} \tag{76}$$

Considering a normalized input, $\tilde{x}(n)$, which has no other effect than scaling the quantization step:

$$\eta_Q \simeq \frac{\langle \mathrm{E}\{\tilde{x}_1(n)\, y_1(n)\}\, \mathrm{E}\{\tilde{x}_2(n)\, y_2(n)\}\rangle}{\langle \mathrm{E}\{y_1^2(n)\}\ \mathrm{E}\{y_2^2(n)\}\rangle^{\frac{1}{2}}} \tag{77}$$

This result would match [3] in the particular case of a wide-sense stationary output, where the instantaneous statistics are constant and equal for both signals. In general, the different phase and/or frequency at the frequency converter makes the instantaneous statistics differ from one signal to the other.

The instantaneous variance of the re-quantizer output has been computed in Appendix A:

$$\mathrm{E}\{y^2(n)\} = \left(P - \frac{1}{2}\right)^2 - 2\sum_{m=0}^{M-1}\sum_{q=1}^{P-1} \mathrm{P}_\Delta(m)\, q \left[\mathrm{erf}\left(\frac{q\,\varepsilon - \mu_m(n)}{\sqrt{2}\ \sigma_{\hat{z}s}(n)}\right) + \mathrm{erf}\left(\frac{q\,\varepsilon + \mu_m(n)}{\sqrt{2}\ \sigma_{\hat{z}s}(n)}\right)\right] \tag{78}$$

where ε is the re-quantization step when $x(n)$ has not been normalized, M and P are half the number of levels of the ADC and the re-quantizer, and

$$\mu_m(n) = \left(m + \frac{1}{2}\right)\cos(\omega n + \varphi) \qquad\qquad \sigma_{\hat{z}s}(n) = \sigma_z|\sin(\omega n + \varphi)| \tag{79}$$

The probability of occurrence of an ADC output value is

$$\mathrm{P}_\Delta(m) = \begin{cases} \dfrac{1 - \mathrm{erf}\left(\dfrac{m\Delta}{\sqrt{2}}\right)}{2}, & m = M-1 \\ \dfrac{\mathrm{erf}\left(\dfrac{(m+1)\Delta}{\sqrt{2}}\right) - \mathrm{erf}\left(\dfrac{m\Delta}{\sqrt{2}}\right)}{2}, & m = 0, \dots, M-2 \end{cases} \tag{80}$$

where Δ is the ADC quantization step in RMS units.

As regards the instantaneous input-output cross-correlation [3]:

$$\mathrm{E}\{\tilde{x}(n)\, y(n)\} = 2\sum_{p=0}^{P-1}\left(p + \frac{1}{2}\right)\mathrm{I}_{\tilde{x}}(p;n) \tag{81}$$

where

$$\mathrm{I}_{\tilde{x}}(p;n) = \begin{cases} \displaystyle\int_{p\tilde{\varepsilon}}^{(p+1)\tilde{\varepsilon}} \tilde{x}\, f_{\tilde{x}}(\tilde{x};n)\, d\tilde{x} & p = 0, \dots, P-2 \\ \displaystyle\int_{(P-1)\tilde{\varepsilon}}^{\infty} \tilde{x}\, f_{\tilde{x}}(\tilde{x};n)\, d\tilde{x} & p = P-1 \end{cases} \tag{82}$$

and the marginal PDF of the normalized re-quantizer input follows a Gaussian mixture model, as was described in Appendix A:

$$f_{\tilde{x}}(\tilde{x};n) = \sum_{m=0}^{M-1} \mathrm{P}_{\Delta}(m)\left[\Phi_1(\tilde{x},\tilde{\mu}_m,\tilde{\sigma}_x;n) + \Phi_1(\tilde{x},-\tilde{\mu}_m,\tilde{\sigma}_x;n)\right] \tag{83}$$

where $\tilde{\mu}_m(n) = \mu_m(n)/\sigma_z$ and $\tilde{\sigma}_x(n) = \sigma_{\hat{z}S}(n)/\sigma_z$.

On the other hand, the integral:

$$\int_{L(p)}^{U(p)} \tilde{x}\left[\Phi_1(\tilde{x},\tilde{\mu}_m,\tilde{\sigma}_x;n) + \Phi_1(\tilde{x},-\tilde{\mu}_m,\tilde{\sigma}_x;n)\right] d\tilde{x} = \frac{\tilde{\sigma}_x(n)}{2}\dot{\mathrm{P}}_{\varepsilon}(p,m;n) + \frac{\tilde{\mu}_m(n)}{2}\mathrm{P}_{\varepsilon}(p,m;n) \tag{84}$$

where the integral limits are defined according to (82), and $\mathrm{P}_{\varepsilon}(p,m;n)$ and $\dot{\mathrm{P}}_{\varepsilon}(p,m;n)$ were defined in Appendix A, by (52) and (53) respectively. Therefore,

$$\mathrm{I}_{\tilde{x}}(p;n) = \frac{1}{2}\sum_{m=0}^{M-1} \mathrm{P}_{\Delta}(m)\left[\tilde{\sigma}_x(n)\,\dot{\mathrm{P}}_{\varepsilon}(p,m;n) + \tilde{\mu}_m(n)\,\mathrm{P}_{\varepsilon}(p,m;n)\right] \tag{85}$$

which yields:

$$\mathrm{E}\{\tilde{x}(n)\,y(n)\} = \sum_{p=0}^{P-1}\left(p+\frac{1}{2}\right)\sum_{m=0}^{M-1} \mathrm{P}_{\Delta}(m)\left[\tilde{\sigma}_x(n)\,\dot{\mathrm{P}}_{\varepsilon}(p,m;n) + \tilde{\mu}_m(n)\,\mathrm{P}_{\varepsilon}(p,m;n)\right] \tag{86}$$

The above result has to be computed for the different frequency and phase of both signals, and their product averaged over time. For a comparison with the results in Appendix A, the frequency and phase have to be the same for both signals. Then,

$$\langle \mathrm{E}^2\{\tilde{x}(n)\,y(n)\}\rangle \tag{87}$$

computed according to (86) has to be compared to:

$$\begin{aligned}\frac{1}{\eta_A}\langle \lim_{\rho\to 0}\frac{\partial}{\partial\rho}\mathrm{E}\{y_1(n)\;y_2(n)\}\rangle = \frac{1}{\eta_A}\Bigg\langle\Bigg[\sum_{p=0}^{P-1}\left(p+\frac{1}{2}\right)\sum_{l=0}^{M-1}\dot{\mathrm{P}}_{\Delta}(l)\;\mathrm{P}_{\varepsilon}(p,l;n)\Bigg]^2\Bigg\rangle \\ + \Bigg\langle\Bigg[\sum_{p=0}^{P-1}\left(p+\frac{1}{2}\right)\sum_{l=0}^{M-1}\mathrm{P}_{\Delta}(l)\;\dot{\mathrm{P}}_{\varepsilon}(p,l;n)\Bigg]^2\Bigg\rangle\end{aligned} \tag{88}$$

where only the re-quantizer efficiency has been considered. Both expressions yield similar but different results, as will be shown next through the overall quantization.

B.1 Numerical results

This section compares the approximation developed in this appendix with the exact expression in Appendix A. Figure 11 shows the overall quantization efficiency computed through both methods for a 3-bit ADC and a 2-bit correlator, without. Both methods yield very similar results, and perhaps the most notable differences are the higher maxima in the approximate method for smaller re-quantization steps, but smaller for the maximum at a re-quantization step of 3. The difference between the methods is plotted in Figure 12. Results show a higher error around the maximum. Depending on the stripe, the error can be as high as 6%. There is not a clear trend across different stripes.

Figure 13 compares both methods for the case where both signals are shifted in frequency. As the statistics become more Gaussian for both signals, the approximate method attains better accuracy. This is corroborated by a lower maximum error of 1.5% (see Figure 14). In addition, from the similarity between Figure 12 and Figure 14, it seems that the error is mainly due to the discrete component of the input. The change towards a "more Gaussian" distribution makes the errors smaller and smoother (somehow smeared), which is logical from the consideration that the source of inaccuracy resides in the correlation between one signal and the quantization noise from the other signal for non-Gaussian signals.

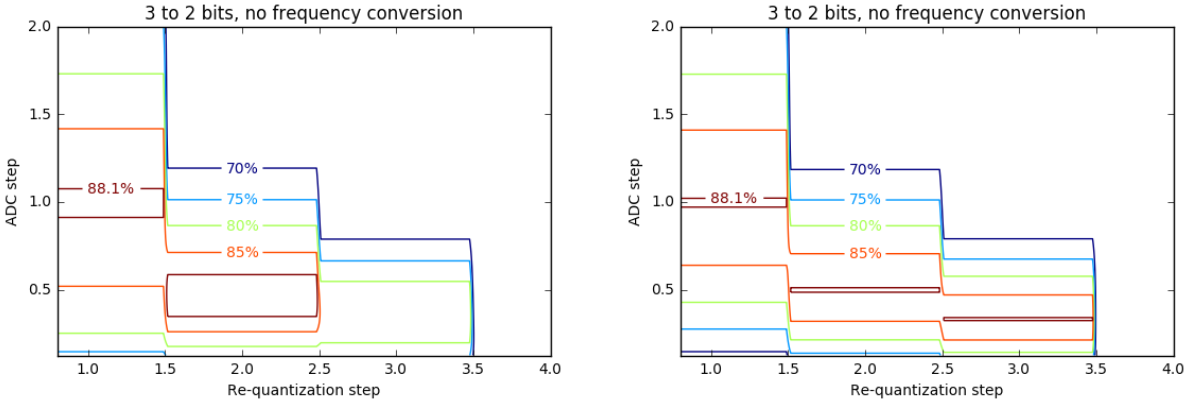

(a) Approximate *(b) Exact*

Figure 11. Overall quantization efficiency using a 3-bit ADC and a 2-bit correlator. No frequency shift is performed on the baseband pair.

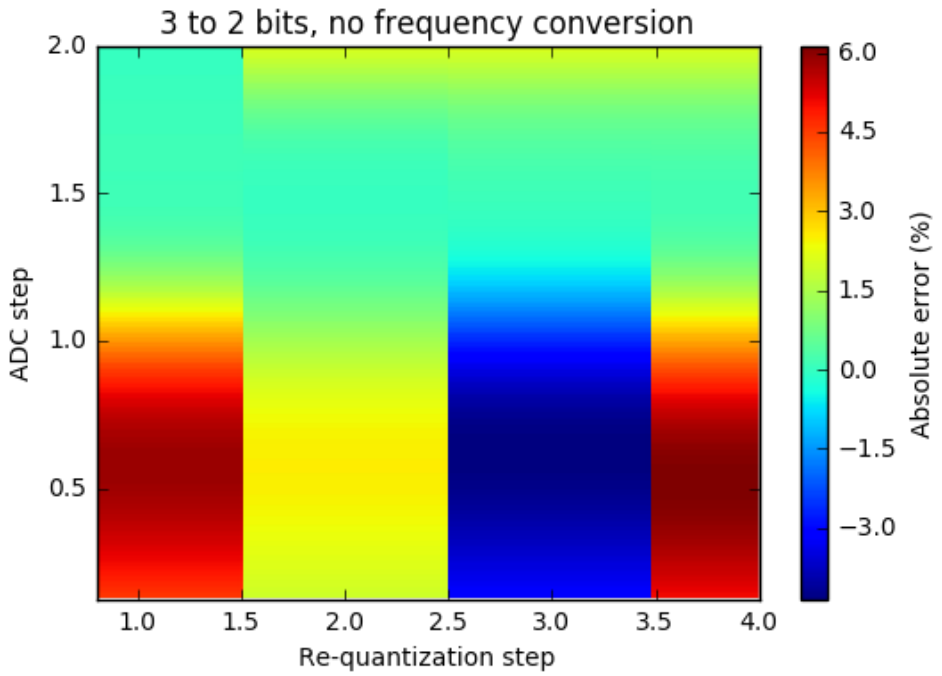

Figure 12. Absolute error in the computation of the overall quantization efficiency through both methods. Positive values stand for a higher value for the approximate method in this appendix. No frequency converter is used.

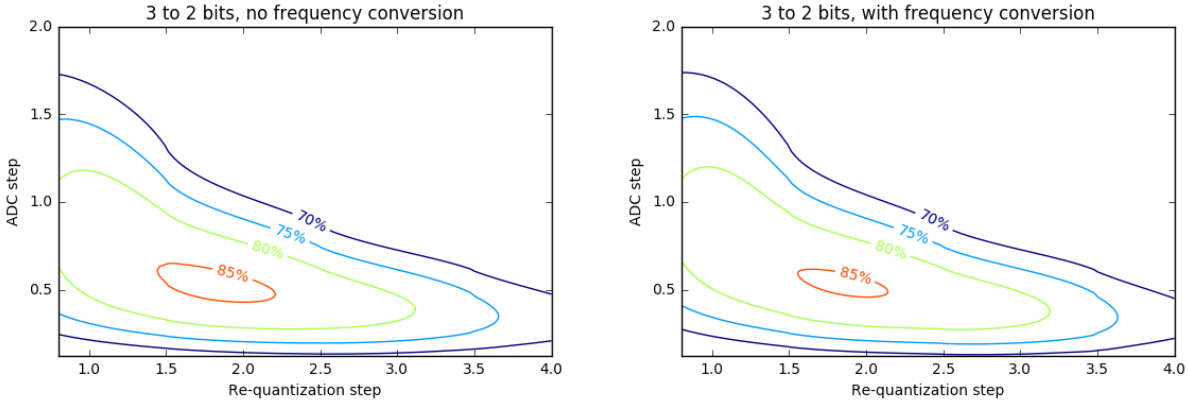

(a) Approximate *(b) Exact*

Figure 13. Overall quantization efficiency using a 3-bit ADC and a 2-bit correlator. Both basebands are frequency shifted prior to re-quantization.

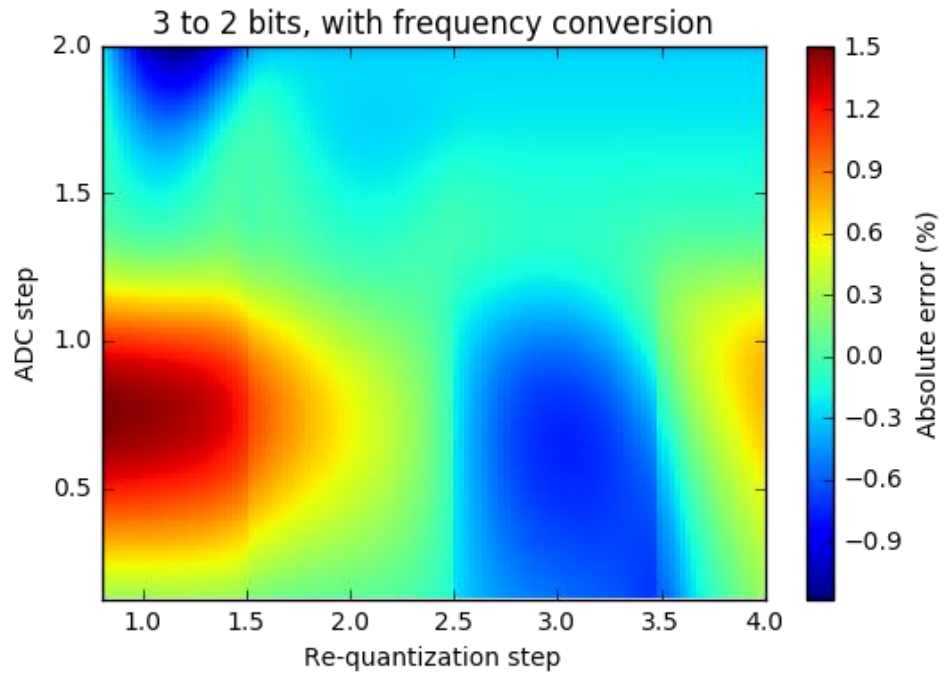

Figure 14. Absolute error in the computation of the overall quantization efficiency through both methods. Positive values stand for a higher value for the approximate method in this appendix. Both signals are shifted in frequency.

Appendix C. Results for a 3-bit ADC and 4-bit correlator

C.1 No frequency converter

Figure 15 represents the contour lines of the quantization efficiency as a function of the ADC's and the re-quantizer's quantization steps. Contrary to the results for a 2-bit correlator, the plot shows a single absolute maximum, 96.256%, at the expected ADC quantization step, viz. 0.586, and a re-quantization step near 1. A close local maximum is obtained for the same ADC step but half the re-quantization step. However, the final value assignation after the re-quantizer in that case is slightly different from linear, which causes the efficiency loss.

C.2 Both basebands are shifted in frequency

The quantization efficiency for this case is plotted in Figure 16. The results are qualitatively very similar to those obtained for the 2-bit correlator. In this case, the maximum efficiency is 95.249%, obtained for an ADC quantization step 0.579, and a re-quantizer step 0.553. These values are slightly smaller than the optimum quantization steps for FDM, 0.586 and 0.561 for the ADC and the re-quantizer, respectively.

C.3 Only one baseband is shifted in frequency.

Finally, the efficiency for the case where only one baseband undergoes a frequency conversion can be approximated as the geometric mean of the two previous cases. The result is shown in Figure 17. The global maximum is now 95.500% and locates near the maximum in Figure 16, namely at 0.560 and 0.558, for the ADC and re-quantization steps, respectively. A close value can be obtained with a re-quantization step equal to 0.875. All these results can be well understood from the previous considerations.

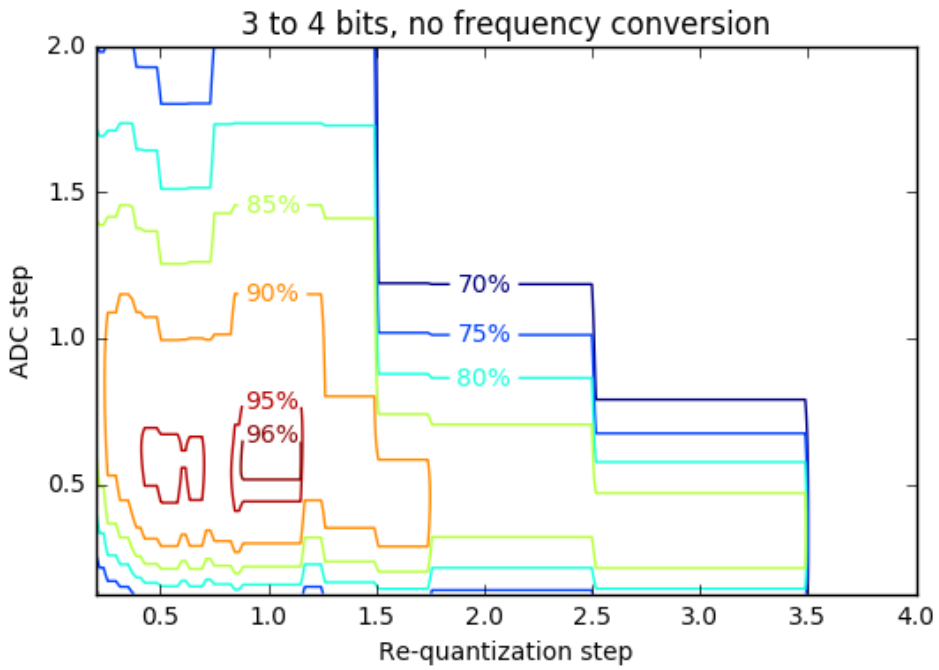

Figure 15. Overall quantization efficiency using a 3-bit ADC and a 4-bit correlator. No frequency shift is performed on the baseband pair.

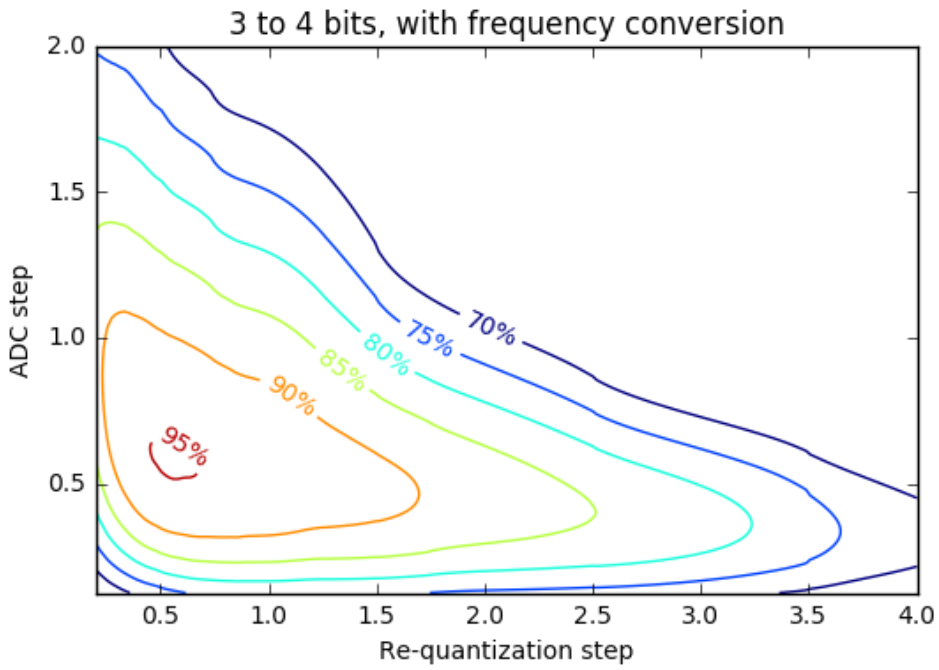

Figure 16. Overall quantization efficiency using a 3-bit ADC and a 4-bit correlator. Both basebands are frequency shifted prior to re-quantization. The maximum efficiency is 95.25%.

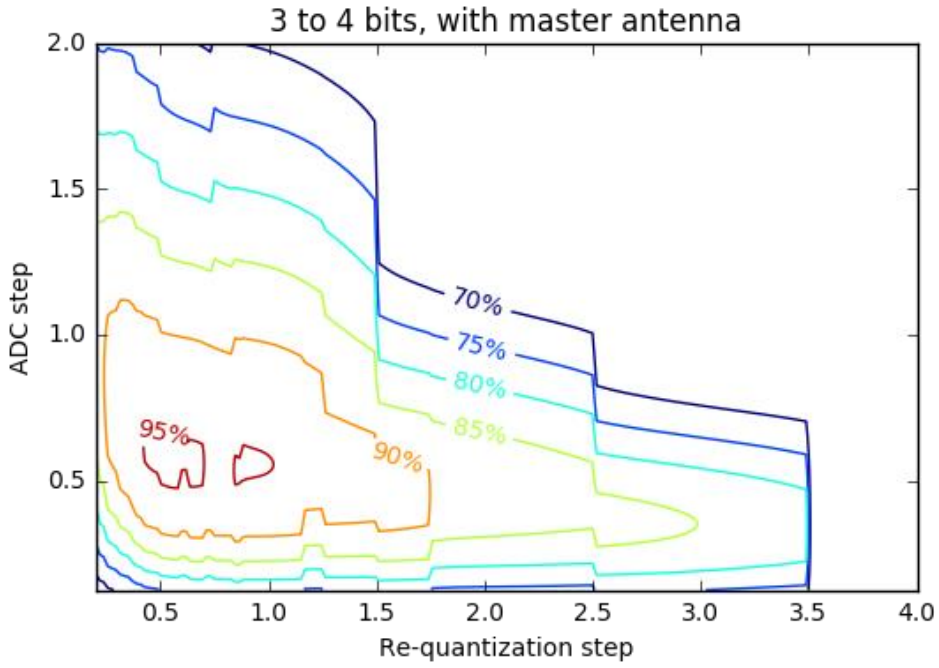

Figure 17. Overall quantization efficiency using a 3-bit ADC and a 4-bit correlator. Only one baseband is shifted in frequency after the ADC. The maximum efficiency is 95.50%, for a re-quantizer step 0.558.

Appendix D. Dependence on phase and frequency

Results show that the variation of quantization efficiency with the phase or frequency of the complex sinusoids at the frequency converters is, in general, very small. For example, Figure 18 plots the difference in quantization efficiency as the phase difference between the two frequency converters vary. The results have been computed through the approximate method in Appendix B for the optimum quantization steps. The period of the sinusoid is 128 samples, so the time averages are taken over one period. As can be seen, the method reveals a maximum deviation under 0.016%, which is negligible. The approximate computation method yields a quantization efficiency at the optimum quantization steps around 0.3% higher than the exact method.

On the other hand, the quantization efficiency does depend on the period of the sinusoid at the frequency converters. After all, not shifting in frequency can be seen as using a sinusoid of period 1 sample (a frequency equal to 1) and phase zero. For a sinusoid of period 2 samples and phase zero, the input to the re-quantizer is still discrete, so the efficiency is the same as if no frequency converters are used. As the period increases, the efficiency converges to the value indicated for long periods (small frequency assumption). This is shown in Figure 19 as a function of the sinusoid period, or Figure 20 as a function of frequency. In the latter case, the frequency is multiple of 2^{-b} ($b = 10$ in this example), following traditional FPGA implementation of direct digital synthesizers. In both figures, the exact method has been used to compute the efficiency, and the phase at the frequency converters is zero.

A final caveat: the independence from phase only applies to small frequencies greater than zero. Obviously, a $\pi/2$ phase change at frequency zero converts the discrete distribution to a

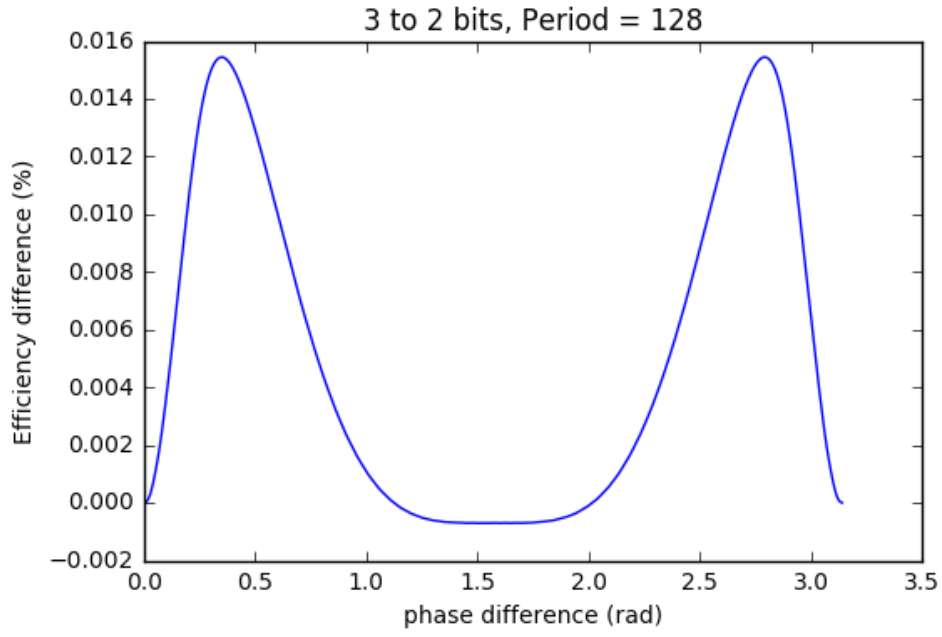

Figure 18. Difference in quantization efficiency as a function of the phase difference with respect to no phase difference. 3-bit ADC, 2-bit correlator.

Gaussian one, as only the Hilbert transform is at the re-quantizer input. Therefore, the efficiency reduces to that of FDM. This dependence will remain for small periods as well.

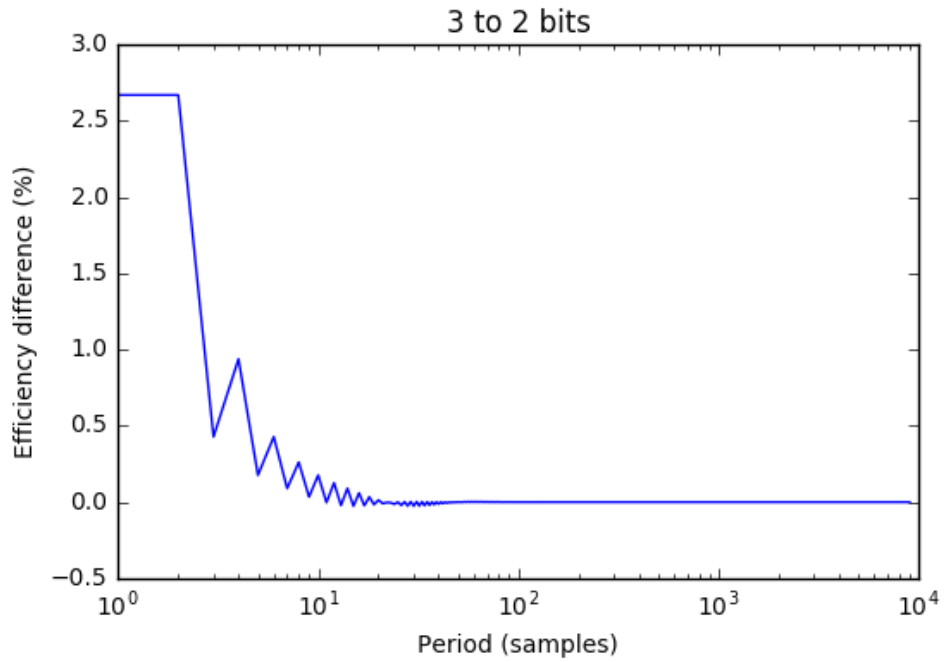

Figure 19. Difference in quantization efficiency as a function of the sinusoid period with respect to long periods. 3-bit ADC, 2-bit correlator.

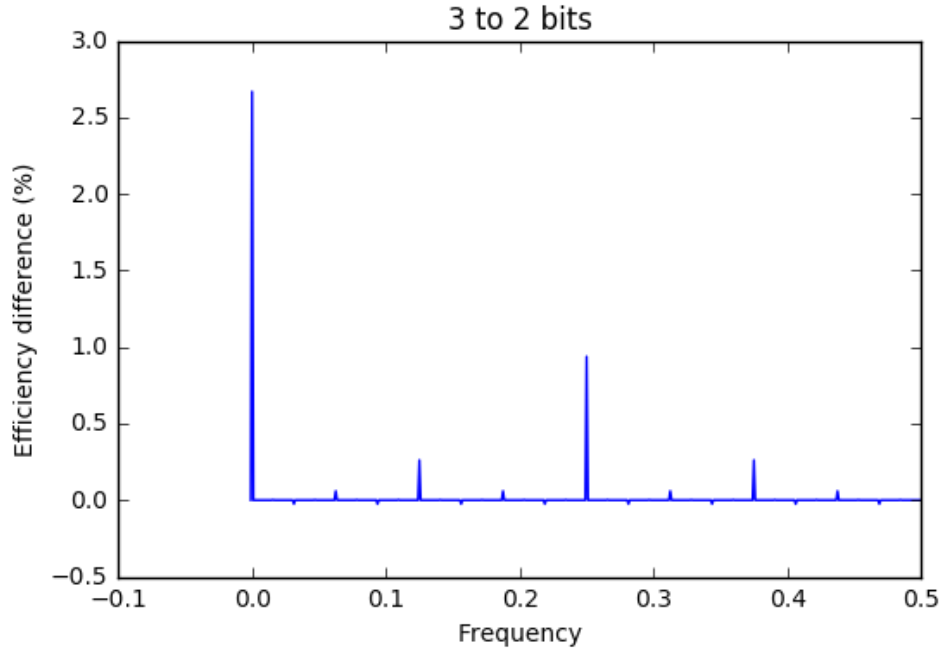

Figure 20. Difference in quantization efficiency as a function of frequency with respect to the first non-zero frequency (1/1024) . 3-bit ADC, 2-bit correlator.